EFFECTS OF IMPACT VELOCITY AND STRESS CONCENTRATORS IN TITANIUM ON FAILURE BY ADIABATIC SHEARING

Final Technical Report
(July17/2000 – Sept.17/2001)

Principal Investigator: J.R.KLEPACZKO

UNITED STATES ARMY EUROPEAN RESEARCH OFFICE
LONDON, UK

CONTRACT N°: N68171-00-M-5984

R&D 9022-AN-01

Contractor:

Laboratory of Physics and Mechanics of Materials
ISGMP, UMR – CNRS 7554
METZ UNIVERSITY
F-57045 Metz, France

REPORT DOCUMENTATION PAGE

Form Approved
OMB N° 0704-0188

1. AGENCY USE ONLY (Leave blank)	2. REPORT DATE	3. REPORT TYPE AND DATES COVERED
	September 18/2001	Final, July 18/2001 – September 17/2001

4. TITLE AND SUBTITLE
EFFECTS OF IMPACT VELOCITY AND STRESS CONCENTRATORS IN TITANIUM ALLOYS ON FAILURE BY ADIABATIC SHEARING

5. FUNDING NUMBERS
N68171-00-M-5984

6. AUTHOR(S)
J.R. KLEPACZKO

7. PERFORMING ORGANIZATION NAME(S) AND ADDRESS(ES)

METZ UNIVERSITY – ISGMP
LABORATORY OF PHYSICS AND
MECHANICS OF MATERIALS

METZ UNIVERSITY
ISGMP-LPMM
ILE DU SAULCY
F-57045 METZ Cedex, FRANCE

8. PERFORMING ORGANIZATION REPORT NUMBER
N/A

9. SPONSORING / MONITORING AGENCY NAME(S) AND ADDRESS(ES)

USA RDSG-UK, AERONAUTICS AND
MECHANICS BRANCH
Dr. Sam SAMPATH

223 OLD MARYLEBONE RD.
LONDON NW1-5th , UK

10. SPONSORING / MONITORING AGENCY REPORT NUMBER

11. SUPPLEMENTARY NOTES

12a. DISTRIBUTION / AVAILABILITY STATEMENT
DISTRIBUTION UNLIMITED

12b. DISTRIBUTION CODE

13. ABSTRACT (Maximum 200 Words)

This Final Technical Report covers the contract period from July 18/2000 to september 12/200. During this period of the Contract all tasks defined by the Statement of Work have been accomplished. Precision machining of the three series of Modified Double Shear (MDS) specimens (the U,V and the sharp notch geometry), total of 62 specimens, has been done in the Laboratory of Physics and Mechanics of Materials (LPMM). Machining and heat treatment of the strikers and the support rings have also been done in LPMM. Since titanium alloys are very sensitive to the onset of the adiabatic shear banding (ASB) it is of great practical interest to study, via experiment and numerical modeling, the effect of stress concentrators on the triggering mechanism of ASB's. The main parameter is the impact velocity or the nominal strain rate in shear. The first series of shear tests was performed on the fast, hydraulic machine. Precise determination of shear characteristics, including failure stress, was performed at the range of the nominal strain rate from 10^E – 3 1/s to $5*10^E$ 2 1/s. The second series of experiments was performed with direct impact loading on MDS specimens of the same geometry, using the air gun, series of strikers and the Hopkinson tube. Range of strain rates from 10^E3 1/s to $4*10^E4$ 1/s has been covered. Digital records of all tests have been analyzed and the rate spectra of the failure stress have been determined. It appears that response of the Ti-6Al-4V alloy is very non-linear as a function of strain rate for all geometry tested. At high strain rates a high rate sensitivity is found, but at very high strain rates (above 10^E4 1/s) a substantial drop of the failure shear stress is observed. Further studies of that effect are needed.

14. SUBJECT TERMS
ADIABATIC SHEAR BANDS, TITANIUM ALLOY Ti-6Al-4V,
STRESS CONCENTRATORS IN IMPACT, DYNAMIC SHEAR FAILURE

15. NUMBER OF PAGES
03

16. PRICE CODE

17. SECURITY CLASSIFICATION OF REPORT	18. SECURITY CLASSIFICATION OF THIS PAGE	19. SECURITY CLASSIFICATION OF ABSTRACT	20. LIMITATION OF ABSTRACT
UNCLASIFIED	UNCLASIFIED	UNCLASIFIED	

EXTENDED ABSTRACT

Since titanium alloys are very sensitive to the onset of the adiabatic shear banding (ASB) it is of great practical interest to study, via experiment and numerical modeling, the effect of stress concentrators on the triggering mechanism of ASB's. The main parameter in this study is the impact velocity or the nominal strain rate in shear combined with different stress concentrators.

This Final Technical Report covers the contract period from July 18/2000 to September 17/2001. Within the framework of this contract the experimental program was continued on the basis of the previous one. In the previous contract, with the same title as this one, the series of the MDS (Modified Double Shear) specimens of Ti-6Al-4V alloy of standard geometry have been tested. The material (Ti-6Al-4V) was delivered by the ARL-Aberdeen, MD and the specimens were machined in the Laboratory of Physics and Mechanics of Materials (LPMM) in Metz. As a result of tests on standard specimen geometry all material constants in a precise constitutive relation have been identified, [1,2,4]. Results obtained with standard MDS specimens served as a basis for further numerical calculations of Adiabatic Shear Bands (ASB). Improved constitutive relations had been used in those calculations, and one paper has been submitted in Jan./2001 to International Journal of Impact Engineering. [4].

Within the framework of this contract the ARL–Aberdeen supplied again the Ti-6Al-4V and three different specimen geometries were machined in LPMM-Metz. Those geometries have different stress concentrators, type "U", "V" and "I" (sharp notch). For every specimen geometry over 20 specimens were made. The most difficult was production of the "I" notch. An electro-erosion technique was used to cut such notch.

At the first stage of the Project the experiments performed for all three geometries were limited to tests with relatively low strain rates in shear, from 10^{E}-3 1/s to 10^{E}2 1/s A fast, hydraulic universal testing machine, together with a special device to fix and load specimens were used. The device has its own gage system to measure the axial force and displacement precisely as a function of time, [3]. It was found that the failure stress of this titanium alloy is not so sensitive in this range of strain rates to stress concentrators.

The LPMM-Metz has developed under previous contracts, partially granted by the European Research Office of the US Army, a unique experimental technique which enables impact shear testing of materials within a wide range of strain rates, the impact range covers strain rates from 10E3 1/s to ~10E5 1/s, [3]. This technique has been applied to perform experiments with three geometries of specimen, that is "U", "V" and "I", with different stress concentrators. The main task was to find the role of stress concentrators in Ti-6Al-4V in triggering ASB. Impact velocities were varied within the following limits: 10 m/s < V < 90 m/s (nominal strain rates: $5*10^3$ 1/s < Γ < $4.5*10^4$ 1/s. The tests performed on U, V and I geometry has served as a basis for further analyses to identify failure criteria based on the concept of effective strain or on concept of the strain energy density. Digital records of all tests have been analyzed and the rate spectra of the failure stress have been determined. It appears that response of the Ti-6Al-4V alloy is very non-linear as a function of strain rate for all geometries tested. At high strain rates a high rate sensitivity is found, but at very high strain rates (above 10^{E}4 1/s) a substantial drop of the failure shear stress is observed. Further studies of that effect are needed.

Refernces

[1] J.R.Klepaczko, Shear Testing of Ti-6Al-4V Alloy at High Strain Rates, up to $6*10^{E}4$ 1/s, Proc. Conf. on Shock-Wave and High-Strain-Rate Phenomena, EXPLOMET 2000, Albuquerque, NM, (2000), in print.

[2] J.R.Klepaczko, Behavior of Ti-6Al-4V alloy at High Strain Rates, Shear Testing up to $6*10^{E}4$ 1/s and Failure Criterion, Proc. Int. Conf. DYMAT 2000, EDP Sciences Les Ulis, J.Phys. IV France **10** (2000), Pr9-191.

[3] J.R.Klepaczko, An Experimental Technique for Shear Testing at High and Very High Strain Rates, the Case of Mild Steel, Int. J. Impact Engng., **15** (1994), 25.

[4] A.S.Bonnet-Lebouvier and J.R.Klepaczko, Numerical Study of Shear Deformation in Ti-6Al-4V at Medium and High Strain Rates, Critical Impact Velocity in Shear, Int. J. Impact Engng; (2001), in print.

Research reported in this document has been made possible through the support and sponsorship of the US Government through its European Research Office of the US Army. This Interim Report is intended only for the internal management use of the Contractor and the US Government.

CONTENTS

1. Introduction and Objectives

In this research program experimental and numerical studies on the effects of different impact velocities (nominal strain rates), involving the shear mode of deformation, and stress concentrators in titanium alloy Ti-6Al-4V were carried out. Since titanium is highly rate-sensitive and it exhibits relatively low rate of strain hardening , its behavior under impact loading leads to an almost instantaneous formation of Adiabatic Shear Bands (ASB). It is of interest to study the substantial differences which occur in formation and localization of the ASB's in metals, including titanium alloys, when the initial conditions, like the local stress concentrators and the local rate of shearing are extremely different.

The main purpose of this study which is the second part of the research program on titanium alloy Ti-6Al-4V carried out by LPMM-Metz, was to clarify, using experiments and numerical methods, the role of short-time local plastic fields with thermal coupling and the local high strain rates in development of impact failure in shear. Some time ago a new failure criterion based on the strain energy density has been included in FE numerical code. It has been shown in the first part of this research program [1] that the local failure criterion based on the maximum localization strain (effective strain in 3D problems) assures relatively good predictions of fracturing by FE codes in shear mode of deformation Finally, within the framework of the previous contract [1], the Modified Double Shear (MDS) experimental technique with the standard specimen geometry, [2,3,4], was used to determine shear stress vs. shear strain characteristics of titanium alloy T1-6Al-4V for a wide range of strain rates. A fast hydraulic machine, and the direct impact technique with impact velocities from 1 m/s to 100 m/s were applied in the previous test program (strain rate range from 10^{E}-3 to $5*10^{E}4$ 1/s with the standard MDS specimen geometry). The Critical Impact Velocity in shear was also analyzed by analytic and numerical methods. [5,6,7,8].

Mechanical tests at high strain rates as well as ballistic tests performed on pure titanium and titanium alloys, show its extreme sensitivity to formation of the ASB's, [9,10]. Consequently, studies of ASB's in titanium alloys are the most important part of the research for improvement of titanium performance against impact.

The adiabatic shear banding in metals have already been studied for some time, including experiment, analytic solutions and numerical calculations. Although some

data are available as to specific extreme conditions when and where the ASB's are formed, no systematic study exists in the open literature on the effect of the nominal velocities of shearing, or impact velocities, on the critical conditions for the onset and evolution of catastrophic thermoplastic shear. It appears in addition that stress concentrators in shear very easily trigger ASBs. It may be mentioned that ASB's, with or without phase transformation, often act as the sites of fracture initiation in Mode II, [11,12,13].

Fast plastic shearing can be studied by using experimental techniques like the Split Hopkinson Torsion Bar (SHTB or Kolsky torsion apparatus). Because the mass velocity in propagation of elastic torsion waves in bars or tubes is limited, the range of the nominal strain rates in SHTB is limited to strain rates in shear from ~$5*10^{E}2$ 1/s to ~$2*10^{E}3$ 1/s. ASBs can also be studied, as a hybrid approach, by numerical methods, including the finite differences [14,15] or finite elements methods [6,7,8].

Because of natural limits imposed on SHTB scheme, a few years ago an original experimental technique for fast shearing has been developed in Laboratory of Physics and Mechanics of Materials (LPMM) in Metz, [2,16]. This experimental technique is based on the double shear principle. The technique combines several positive features not available with other setups. The scheme of the double shear technique is shown in Fig.1. Because the theory and details of this experimental technique is given elsewhere [2], here only a brief description is offered. Fig. 1 shows the principles.

The direct impact of a projectile is applied to deform plastically up to failure the MDS specimen, for example of standard geometry, as it is shown in Fig.2. In this way the rise-time during the specimen loading has been substantially reduced (~2 μ s). For example in comparison to the Split Hopkinson Pressure Bar (SHPB) technique the typical rise time is ~20 μs, and for SHTB the typical rise time is ~50 μs. Flat-ended strikers of different length made of maraging steel and of diameter D_p = 10.0 mm are launched from an air gun with predetermined velocities V_0 , 1.0 m/s < V_0 < 200 m/s. The impact velocity is measured by the setup with three sources of light L , fiber optic leads 1,2,3 and three independent photodiodes F which activate two time counters TC1 and TC2. The time intervals of dark signals from the photodiodes generated during the passage of a projectile are transmitted to

the start/stop gates of the time counters. The impact velocity can be precisely measured.

Axial displacement $U_X(t)$ of the central part of the DS specimen is measured as a function of time by an two channel optical gauge E, acting as a non-contact displacement gage. The optical gage reacts to the axial movements of a small black and white target cemented to the middle part of the MDS specimen. The second channel can measure displacement of the interface striker/specimen, so the coefficient of restitution can be independently determined.

Axial force which is transmitted by the specimen symmetric supports which are attached to a long Hopkinson tube can be determined as a function of time from the transmitted longitudinal wave $\varepsilon_X(t)$ measured by SR gages T_1 cemented on the Hopkinson tube, DC supply unit A_2 and wide band amplifier A_1. All electric signals (from the optical extensometer and SR amplifier) are recorded by digital oscilloscope DO and next stored in a PC hard disk for further analyses.

The direct impact configuration of experimental setup permits for a wide variation of the nominal strain rate in shear, typically from 10^3 1/s to 10^5 1/s. The direct determination of the axial displacement permits also for a more exact evaluation of the deformation history, a very important piece of information in development of ASB's. So far more than a thousand tests have been performed with this technique, including variety of armor steels, VAR 4340 steel 50-52 HRC, aluminum alloys and shock-resistant polymers.

In conclusion, the direct impact technique available in LPMM - Metz constitutes a reliable test method to study the impact shear in the wide range of velocities.

The numerical methods, like the finite differences and the finite elements are advanced enough and they are very useful in studies of the ASB's. In addition to the finite difference method applied in LPMM-Metz to study the steady-state formation of the ASB's in 1018 steel, [14], recently, the FE code (ABAQUS implicit and explicit schemes) has been applied to study the Critical Impact Velocity (CIV) in shear, [6,7,8]. In this research program a complete dynamic approach with the elastic-plastic wave propagation and a new constitutive relations, including thermal coupling, has been applied to study CIV in shear for Ti-6Al-4V alloy. The CIV in shear can be used as a new material constant, [4,5,6,8], similar to Kàrman's Critical Impact Velocity in tension [17,18]. The existence of the CIV in shear has far

reaching consequences in fragmentation, [19,20]. Recent numerical studies have confirmed experimental observations as to existence of the CIV in shear for 1018 steel, VAR 4340 steel 52 HRC and Ti-6Al4V [7,8]. The CIV in shear triggered by plastic wave trapping, [21], causes that the energy needed to trigger an ASB is much lower when the local shearing velocity exceeds the CIV. This is a new important fact to be studied for different materials including titanium alloys. The physics of this phenomenon is now understood much better.

2. Technical Objectives

Since titanium and titanium alloys are even more sensitive to the onset of the ASB's in comparison to steels, it is of great practical interest to study, via experiment and numerical methods, the effect of stress concentrators on the triggering mechanisms of ASB's in those metallic materials. Such study could advance the state of the art in this area. A relation must be sought between titanium properties, imposed conditions in the form of different loading rates (impact velocities), stress concentrators and development of the ASB's. Also the CIV should be studied in titanium, including experiment and numerical approach. A correlation should be sought between susceptibility to catastrophic thermoplastic shear and material properties, including CIV, including defects that initiate the localization.

The unique aspect of this research lies in application of an original and unique experimental technique developed in LPMM-Metz from one side, and an experience already gained in complete numerical analyses of the ASB's by the FE method. It is hoped that this research will have a practical significance in application to more precise design of structures against direct impact and perforation.

The main purpose of this research program was to gain more information on the role of stress concentrators and rate effects in triggering of adiabatic shear bands (ASB) and failure. In pursuit of these goals, experimental studies on the effect of stress concentrators and impact velocities have been undertaken. The materials tested was Ti-6Al-4V. On the other hand, numerical calculations with more realistic boundary conditions have been performed.

In order to clarify the problems mentioned above the first step was clarify the effect stress concentrators in the standard MDS geometry [1,22,23]. The Finite Elements (FE) calculations for the MDS specimen reported in [2,3] have shown

existence of the stress concentrators around the corners present in the standard geometry.

To study further the effect of stress concentrators at different loading rates on formation of the ASB's four different specimen geometry with increasing stress gradients were tested.

The second specific objective involving a more realistic initial conditions imposed during experiments on the MDS specimen, was to clarify the effects of plastic waves, more specifically existence of the Critical Impact Velocity (CIV) in shear [4,5,6, 7,8]. The FE technique has been applied for this purpose [7,8].

The research program included the following scopes:

(1) Precision machining of the three series of Double Shear (DS) specimens with three stress concentrators, "U" - geometry, "V" - geometry and "I" - geometry (sharp notch) of Ti-6Al-4V. The machining was done in LPMM-Metz. Three specimen geometries are shown in Fig.3. The ligament as well as the thickness were the same for all geometries. The width of the fine notch was 0.5 mm, that is "I" geometry, and the notch was cut by the electro-erosion technique;

(2) Three series of DS specimens, each of 20 specimens, were made;

(3) A series of Marval 18 (maraging steel) strikers were machined and heat treated;

(4) The first series of experiments was performed with three specimen geometry on the fast, hydraulic universal testing machine. Precise measurements of shear characteristics were done for each test. The range of strain rates was given above.

(5) The second series of experiments was performed with the same specimen geometry with the direct impact experimental technique. The range of strain rates was given in the previous part of this Report;

(6) Digital records (oscillograms) from all tests have been analyzed and the force vs. displacement data have been obtained. Such experimental results have served as a source for further analyses discussed in the following parts of this Report;

(7) The Ti-6Al-4V plate, in order to produce specimens, has been delivered by ARL-AMSRL-WM-TA, [24].

Those task have been completed as the scope of the Statement of the Work in the Contract N68171-00-M-5984 (Reference Number: R&D 9014-AN07).

3. General Information on Ti-6Al-4V

Titanium and its alloys have proven to be technically superior and cost-effective materials for a wide variety of applications like aerospace, marine and armament. Titanium and its alloys are immune to corrosive attack. The key to its cost-effective use is to utilize its unique mechanical properties.

One of the most utilized titanium alloys is Ti-6Al-4V, Grade 5 alloy. This α-β alloy is the workhorse alloy of the titanium industry. The alloy is fully heat-treatable in section sizes up to ~25 mm, and can be used up to about the absolute temperature 673 K (400°C) with a small reduction of the mechanical characteristics. This alloy has specifications: DIN 3.7165 and the USA MIL-T-9047 and MIL-T-9046 AB1/2.

The mean physical data are:

1. Specific Gravity	4.43 g/cm^3
2. Melting Range	1922 +/- 15 K (1649 +/- 15°C)
3. Specific Heat	0.56 J/g K
4. Thermal Conductivity	7.20 W/m K
5. Beta Transus	1272 +/- 15 K (999 +/- 15°C)

The mean mechanical characteristics at room temperature are:

1. 0.2% Proof Stress	Min. 828 MPa ; Max. 910 MPa
2. Tensile Strength	Min. 897 MPa ; Max. 1000 MPa
3. Elongation over 50 mm	0.10
4. Reduction in Area	0.20
5. Young's Modulus	114 GPa
6. Hardness Rockwell C	36
7. Charpy Impact Energy (V-notch)	24 J

Variation of the 0.2% Proof Stress and Tensile Strength as a function of the absolute temperature, at strain rate ~10^{E}-3, are shown in Fig 4. The temperature variation of the Elongation over 20 mm gage length is shown in Fig.5. It is clear that at temperatures higher than about 700 K the thermal softening is intensified. This information is important because the core temperature in an ASB may exceed substantially this level.

4. Experiments with Different Stress Concentrators

The experimental technique shown in Fig.1 is now a daily practice. The DS specimen with its new standard geometry shown in Fig.2, which prevents plastic deformation and rotation of the supports, has been discussed in [3]. The deformed layer of the standard MDS specimen has 2 mm and it initially assures the uniform deformation over the gage length at low nominal strain rates. The MDS specimens are loaded by direct impact using a bar striker, as it is shown in Fig. 1. Typical records of such tests for standard geometry are shown in Fig. 6 and Fig.7. The MDS specimens made of Ti-6Al-4V were loaded respectively by the striker at impact velocity V = 19 m/s (Fig.6) and V = 24.5 m/s (Fig.7). The two channel digital oscilloscope with the sampling rate 1 GHz was triggered by the signal from the optical transducer, channel 1. It is visible that the velocity of the central part of the MDS specimen is almost constant, no vibrations are present.

The transmitted wave is recorded in channel 2. The delay to propagate the elastic longitudinal wave in the Hopkinson tube, from specimen to the strain gage is ~36 μs. A special computer program has been developed to analyze the digital records and to determine force versus displacement data.

Three series of tests (hydraulic machine and direct impact) for different notch geometry have been performed at room temperature on titanium alloy Ti-6Al-4V within a wide range of nominal strain rates in shear, approximately from 10^{-3} 1/s to ~10^{5} 1/s (that is eight decimal orders). The specimen dimensions are shown in Fig.3. The specimens were machined by LPMM-Metz out of an electron beam single melt plate of thickness 25 mm. The plate designated as AR7006 was made with a special processing [15]. The chemical composition of the initial EB ingot was as follows, Wt.% (average values):

Al: 6.28; V: 4.16; O: 0.76 and other elements: Sn: 0.017-0.019; Zr: 0.022-0.024; Ni: 0.032-0.035; Mn: 0.0; Si: 0.0; Cr: 0.024-0.036; Cu: 0.001-0.004; H: 0.007-0.010; C: 0.024-0.026.

Mechanical properties:

Yield Strength	874 MPa
Tensile Strength	909 MPa

The material (titanium alloy) was delivered by ARL-WM-MC. The total number of specimens machined was 60 (20 for each geometry). The specimens were cut in such a way as to assure the shear direction perpendicular to the rolling direction.

Since there is an interest in studying not only the range of high strain rates but the whole strain rate spectrum including lower strain rates, a special device was used to load DS specimens with a complete measurements of force and displacement, [2]. The scheme of this device is shown in Fig.8. The device is equipped with its own measuring system. The axial force F(t) is measured by the load cell 6 with SR-gages and signal conditioner. The net specimen displacements $\delta_1(t)$ and $\delta_2(t)$ are measured by two LVDT-s and two amplifiers. The DS specimen 3 clamped to the support 2 which is loaded by the punch 4. The main support 1 with the device can be fixed to any testing machine, in this case a fast hydraulic machine was used to deform specimens from 10^E-3 1/s to $2*10^E2$ 1/s. The three signals from the device (force plus two displacement signals) and two electric signals from the machine can be stored in the digital form using digital oscilloscopes. The signals F(t), that is the force, and LVDT displacements are next stored in a PC hard disk for further analyses. An example of such record is given in Fig.9. From such test the axial force and the mean axial displacement can be obtained as a function of time. After elimination of time the force versus the mean displacement can be determined, [2,3]. With this device and the hydraulic machine three series of "quasi-static" tests were performed for each specimen geometry. The listing of "quasi static" tests is given in Table 1. The range of the nominal shear strain rate covered is from 10^E-3 1/s to 100 1/s. At every strain rate at least two good tests were performed. The final results for "U", "V" and "I" geometry are shown in Fig.10 in the form of the mean shear stress vs. logarithm of shear strain rate. At higher strain rates the effect of a heat generated during plastic deformation causing thermal softening is noticeable, the point of

maximum nominal stress is stabilized at the level ~550 MPa. It may be noticed that the lowest cross section for all three specimen geometries is approximately the same, so the nominal stress shown in Fig.10 is referred to this cross section.

Second series of experiments was performed for the same three geometries with the direct impact on the Double Shear (DS) specimens, Fig.3, similar as for 4340 VAR steel, [1,22,23], at impact velocities 15 m/s $< V <$ 90 m/s (nominal strain rates: $7.5*10^E3 < \Gamma < 4.5*10^E4$ 1/s). The complete theory of direct impact test on MDS specimen has been published elsewhere, [2]. Some digital records from those experiments are reproduced in figures: Fig.11 to Fig 16. Similarly as in the case of standard geometry the displacement signal starts earlier (movement of the black and white target on the specimen shown in Fig.1) than the signal of the transmitted wave in the Hopkinson tube. The listing of the direct impact tests is given in Table 2. After analyses of records, and elimination of time, the transmitted axial force vs. axial displacement can be determined for a particular impact velocity. The results in the form of maximum nominal shear stress versus impact velocity are shown in figures: Fig.17 to Fig.19. Because the specimens were machined "as received" (no heat treatment after milling), the scatter is quite large. The order of the scatter is similar as for the standard geometry [1] However, the main trends in the specimen behavior can be analyzed. Above impact velocity ~20 m/s (nominal shear strain rate 10^E4 1/s) the nominal shear stress slightly increases for the "U" geometry and the plateau is reached at the level ~1500 MPa. On the contrary, the nominal stress for the "V" geometry shows maximum at ~25 m/s (nominal strain rate $1.25*10^E4$ 1/s) and next a systematic decrease up to the level ~1000 MPa at impact velocity 80 m/s. Behavior of "I" geometry is "in between", the plateau is reached at ~20 m/s which rests constant at the level ~1350 MPa up to ~90 m/s ($4.5*10^E4$ 1/s). Lack of data for impact velocities higher than 90 m/s does not permit to verify a drop of the nominal shear stress at higher impact velocities. All three trends shown in Figs 18 to 20 should be verified by FE code with a failure criterion.

In order to analyze the rate effect the nominal maximum shear stress determined for "U","V" and "I" geometry is plotted as a function of the logarithm of strain rate respectively in Fig.20, Fig.21 and Fig.22. As expected, at lower nominal strain rates the maximum shear stress for all geometries is proportional to the logarithm of strain rate. At strain rate range from $5*10^E3$ 1/s to about 10^E4 1/s the measured

stress increases substantially and at higher strain rates it stabilizes as it is discussed above. Finally, the whole rate spectrum for all three geometries is shown in Fig.23. At this scale the general trend is obvious, the maximum shear stress substantially increases up to a plateau, and at high nominal strain rates a substantial decrease is found. Such behavior is. similar as reported in [35]. Further studies of such behavior would be important

5. Determination of the Failure Energy

In case of fast shearing metals and alloys behave as it is shown in Fig.24. The nominal shear stress increases linearly as a function of the nominal shear strain in the elastic range, plasticity is triggered at the yield point τ_y and next a strain hardening appears. Since large part of the plastic work is converted into heat the material softens and the instability point occurs at the maximum stress. This is the end of stage 1. During stage 2 strain localization occurs in the form of ASB and in stage 3 the localization process is accelerated into the final failure indicated by the black point. Since the process of localization is plotted as a function of the nominal shear strain the local strain at the failure point can be many times higher. When the nominal shear strain rate is increased, or impact velocity increases, the instability point in the adiabatic conditions occurs at smaller strains as it is shown in Fig.25.

Specimen response shown in Fig.24 and fig.25 can be transformed into energy analysis. That is the energy expanded during stages 1, 2 and 3, and the total energy to failure, can be found by integration. It may be seen from Fig.25 that the total energy to failure may not change much because failure may occur at smaller and smaller nominal strains when strain rate is increased.

The energy analysis has been performed for all tests with three geometries "U", "V" and "I". The results are shown in Fig.26 and Fig.27 in the form of the energy up to the maximum force as a function of the logarithm of nominal strain rate for lower strain rate spectrum, and as a function of impact velocity after DS tests. An interesting picture emerges. Since deformed plastically volumes differ for each specimen geometry the energy to failure diminishes in the order of "U" , "I" and "V". The notch acuity in the case of "V" geometry was higher than in "I" geometry and the energy up to instability point is lower for "V" than for "I". The effect of adiabatic heating is the most intense for the "U" geometry. In the case of "V" and "I" the

thermal softening is compensated by a very high local strain rate at the tip of stress concentrators by a very high rate sensitivity.

At high nominal strain rates, Fig.27, the rate sensitivity, and perhaps to some extend inertia (wave propagation) seem to be dominating. The energy at the maximum nominal shear stress increases for all three geometries. Comparison of Fig.26 and Fig.27 indicates a minimum of energy for all stress concentrators around nominal strain rate 10^E3 1/s. The highest increase of energy , around two to six times at the nominal strain rate ~ $4*10^E4$ 1/s, is observed for the "U" notch (impact velocity ~ 80 m/s).

Similar results have been obtained for the total energy to failure. The experimental points are shown in Fig.28 and fig.29, respectively for the lower and the higher rate spectra. In Fig.29 the energies are only slightly higher, indicating that the localization is very fast. However, at high nominal strain rates (DS tests) an increase of the total energy is substantial. For example, the "U" geometry shows about twofold energy increase around maximum which occurs at 50 to 70 m/s (nominal strain rate $2.5*10^E4$ 1/s to $3.5*10^E4$ 1/s). On the other hand the weak maxima of energy can be noticed for all three geometries. The whole rate spectra for both energies are shown in Fig.30 (energy up to maximum stress) and in Fig.31 (the total energy). As it is discussed above a substantial increase of both energies are found within the range of the nominal strain rates 10^E4 1/s $\leq \dot{\Gamma} \leq 4.5*10^E4$ 1/s . At "quasi-static" strain rates of the order 10^E2 1/s the energy for the "U" profile is about 10 J and for the "V" stress concentrator decreases to 5.0 J.

The failure energy dissipated during plastic deformation for the same specimen geometry has also been analyzed for VAR 4340 steel (52 HRC) , [23]. Those results are reproduced in Fig.32 and fig.33. In Fig.32 the whole spectrum of strain rates is shown. The spectrum was obtained via DS experiment. In Fig.33 the numerical results are reproduced which were obtained by FE analysis with the failure criterion based on the effective plastic strain. Comparison of experimental results obtained for VAR 4340 steel and Ti-6AL-4V alloy indicate a substantial differences in behavior of those two materials. When the nominal strain rate, or impact velocity, is increased the energy to break the VAR 4340 steel substantially diminishes for all geometry tested, whereas for Ti-6Al-4V the energy for both cases, that is at maximum force and at failure, diminishes initially up to the nominal strain rate ~10^E3 1/s and next increases up to relatively high values. For example, at the

nominal strain rate ~3.2*10^{E}4 1/s the energies to failure for VAR 4340 steel vary from ~1.5 J to ~3.5 J depending on the stress concentrator, whereas the range of energies to failure for Ti-6Al-4V at the same strain rate vary from ~28.0 J to ~80.0 J. Those large differences are fundamental and should be clarified in the future. They indicate on *totally different physical processes* of adiabatic failure in steels and titanium alloys.

The energy analysis provides a very important information for evaluation of the local failure criteria by different stress concentrators. Some local criteria are discussed in the following part of the Report.

6. Constitutive Relations for Ti-6Al-4V

After careful analyses of experimental data available in the open literature for Ti-6Al-4V alloy and the results obtained with the MDS technique (standard specimen), the following explicit form of the constitutive relation has been developed for application in numerical codes

$$\tau = \frac{\mu(T)}{\mu_0}\left[B\left(\frac{T}{T_0}\right)^{-\nu} (\Gamma_0 + \Gamma_p)^{n(T)} + \left(1 - \frac{T}{D}\log\frac{\dot{\Gamma}_0}{\dot{\Gamma}}\right)^{m}\right] \qquad (1)$$

where B, μ_0, ν, n, m are respectively, the modulus of plasticity, the shear modulus at $T = 300$ K, the temperature index, the strain hardening exponent and the logarithmic rate sensitivity, $T_0, \Gamma_0, \dot{\Gamma}_0$ and D are normalization constants. This constitutive relation was used earlier to study ASB's by the FE code ABAQUS, [25], for 4340 steel [1,6,7,24].

The temperature change of the shear modulus in Eq.(1) is given by

$$\mu(T) = \mu_0\left(1 - AT^* - CT^{*2}\right); \quad T^* = T - 300 \qquad \text{T} > 300\ \text{K} \qquad (2)$$

where A and B are constants, and $T^* = T - 300$ K is the modified temperature. In principle, this version of constitutive equations can be applied at RT and temperatures above 300 K.

Since it is known that the rate of strain hardening in metals and alloys is temperature dependent and it diminishes with an increase of temperature [26]. The strain hardening exponent n was assumed as a linearly decreasing function of the homologous temperature, [26]

$$n(T) = n_0\left(1-\frac{T}{T_m}\right) \tag{3}$$

where n_0 is the strain hardening exponent at $T = 300$ K, and T_m is the melting point. This modification was found essential for very high strain rates. .

The structure of the constitutive relation, Eq.(1), has some elements based on the materials science approach. First of all the level of stress is normalized by $\mu(T)/\mu_0$ which takes into account the thermal softening of the crystalline lattice. The first expression in Eq.(1) in the brackets is simply the internal stress and the second one is the rate and temperature-dependent effective stress, for example [27,28].

The procedure of how the constitutive relations have been developed is not discussed here, [1]. Total number of constants in Eqs (1), (2) and (3) is 12 and they are given in Table 3. Recently, the constitutive relations have been optimized for Ti-6Al-4V, [29]. Table 3 contains the optimized constants.

Since a large part of the plastic work is converted into heat the temperature of a material increases when plastic deformation advances. The balance of energy with the heat conduction leads to the following relation

$$\beta\tau\frac{\partial\Gamma}{\partial t} = \rho C_V\frac{\partial T}{\partial t} - \lambda\frac{\partial^2 T}{\partial y^2} \tag{4}$$

where y is the axis of the heat conduction, β is the coefficient of energy conversion, for example [15,30], ρ, C_v and λ are respectively the mass density, the specific heat and the heat conductivity (Fourier constant). It has been recently found for Ti-6Al-4V, [30], that the coefficient of stored energy β depends on strain rate. The relation of how β changes as a function of strain rate is given below

$$\beta = \beta_0 - \alpha\log\left(\frac{\dot{\Gamma}_0}{\dot{\Gamma}}\right) \qquad \beta > 0 \tag{5}$$

When the process is entirely adiabatic, $\lambda = 0$, (no heat conduction) the heating is uniform in an elementary volume. All material constants for the thermal coupling analyses, the total is 5, are given in Table 4 of this Report. If the heat conduction is negligeable an increase of temperature in the adiabatic process of plastic deformation can be calculated after integration of Eq.(4), and if the temperature sensitivity of the flow stress ν is already known the thermal softening of the flow stress can be finally calculated [1].

Thermal characteristics which are discussed above permit for numerical simulations of all temperature-coupled problems as purely adiabatic as well as with the heat conduction. The code ABAQUS includes those thermal-coupling problems in FE procedures.

7. Failure Criteria for Shear and Spalling

7.1 Failure Criteria for Adiabatic Shear

The main purpose of studying failure and fracture processes at high loading rates is to clarify, using experiments and numerical methods, the role of short-time local plastic fields with thermal coupling, and the local high strain rates, in development of impact failure. A new failure criteria based on the strain energy density or effective plastic strain have to be included in FE numerical codes.

The instability strain can be determined in many ways. The first possibility is to use the condition of maximum force in shear, that is $(\partial\tau/\partial\Gamma)=0$. This condition can be applied to experimental $\tau(\Gamma)$ curves as well as to theoretically determined adiabatic $\tau(\Gamma)_A$ curves at different strain rates.

Another possibility is to measure the slopes of specimen contours on the shear sides. Deformed MDS specimen (standard geometry) of Ti-6Al-4V is shown in Fig.34, [29].. The slopes that are measured with a microscope are indicated by broken lines. Such determination of the instability strain has been applied to all standard specimens tested at high strain rates, the result is shown in Fig.35. As expected, the mean values (black points) show that the instability strain diminishes as a function of strain rate up to strain rate ~10^E4 1/s and next increases. The minimum instability strain estimated by this method is ~0.045.

The instability strain has also been estimated numerically by application of the maximum shear stress condition. The result is shown in Fig.36 in the form of the solid line superimposed on the experimental data from Fig.35. A shallow minimum is also found with the correct level of the minimum localization strain, ~0.04.

Experimentally determined, via oscillograms, the instability and failure strains for the whole range of strain rates are shown for VAR 4340 steel in Fig.37 and Fig.38 as a function of the logarithm of strain rate. It is clear that for VAR 4340 an increase of strain rate accelerates instability and failure strain. This trend is continued up to strain rate ~10^E4 1/s, as it is shown in Fig.37 for the higher range of strain rates, and next the instability strain shows a light tendency to increase. The decrease of the instability strain is due to adiabatic heating, it is also leading to an early strain localization and failure by ASB's. A more general discussion of such behavior can be found in the literature, for example [4,31]. The prediction of the instability strain based on the constitutive relation developed for VAR 4340 is discussed in another Report for the US Army, [23].

Comparison of the minimums of the instability strains for VAR 4340 steel (Fig.37 and Fig.38) and Ti-6Al-4V alloy (Fig.35) indicates for four times larger instability strain in the case of Ti alloy (~0.045) than in the case of steel (~0.01).

At high nominal strain rates, as it is mentioned above, the plasticity in the shear zone is substantially reduced. It is presumed that for VAR 4340 steel a quasi-brittle behavior dominates (Fig.37). Of course, this is caused by adiabatic coupling and stress concentrators which generate locally a very high strain rate, [1]. The behavior reported in Fig.35 indicates that the specimens of the Ti-6Al-4V tested at very high nominal strain rates, higher than 10^E4 1/s, are overall "less brittle" in comparison to the tests performed at lower nominal strain rates ~10^E4 1/s. In order to calculate numerically by FE an evolution of the plastic zones and failure, it is necessary to introduce *a local failure criterion* . A local criterion can be used with or without fracture mechanics principles (stress intensity factor or J-integral). In the present study a more simple approach was adopted, that is a specific value of the failure shear strain. This value can be determined as proportional to the instability strain defined by $(\partial\tau/\partial\Gamma)_A = 0$ in the adiabatic conditions of deformation with the proportionality coefficient a . Thus the local failure criterion adapted in this study can be written as follows

$$\Gamma_1 = \alpha \, \Gamma_i \qquad (6)$$

with $\alpha >> 1.0$. Values of coefficient α were estimated by an inverse technique using FE code for both VAR 4340 steel, [23], and for Ti-6Al-4V alloy, [1,8]. The result of estimation is shown in Fig.39 for VAR 4340 steel. The value of α can be estimated as ~12, since the instability strain at the minimum is ~0.01 and the failure strain found by FE technique is ~0.12. The result of similar estimation for Ti-6Al-4V is shown in Fig.40. This early estimation with the first version of the material constants predicts the minimum of the instability strain as ~0.024, almost twice lower than resent numbers. However, the estimation of the minimum of the failure strain yields correct value of the failure shear strain ~1.23, Fig.40. So the improved value of α is ~29.3. In the previous version $\alpha \approx 50$, [8]. In conclusion, the absolute value of the failure shear strain ($\Gamma_c \approx 1.23$) for Ti-6Al-4V is more than ten times larger than for VAR 4340 steel ($\Gamma_c \approx 0.12$). The numbers given above explain to some extend fundamental differences between those two materials.

Some specimens broken in extreme conditions, that is those loaded at very high strain rate, were examined with the Scanning Electron Microscopy (SEM), [1]. When the loading rate is high, for example impact velocity ~40 m/s (nominal strain rate $2*10^E4$ 1/s), many shear dimples are visible, together with some patches of a smeared metal where the temperature is probably a large fraction of the melting point. At the impact velocities 98 m/s and 107 m/s, (nominal strain rates $4.9*10^E4$ 1/s and $5.37*10^E4$ 1/s) the smear patches are much larger, and mixed with micro-dimples, indicating for a substantial increase of the local temperature, probably close to the melting point. The size of dimples is from 1 to 10 micrometers. It is difficult to state whether the broken ASB's are transformed or not since the perpendicular observation was not performed. As a whole the micro-mechanism of impact shearing in Ti-6Al-4V does not differ much from those observed in other industrial alloys, for example 4340 VAR steel [23].

7.2 Failure Criteria for Spalling

During penetration of KE projectiles against metallic targets, mostly plates, the a shock wave propagates through the thickness and later is reflected as a tensile wave. Superposition of the incident shock wave (compression) and the reflected one

(tension) develops a high tensile stress *inside* the target plate. This tensile wave is so high that causes tensile failure called spalling. During recent decades a substantial progress has been made in understanding fracture mechanisms under very short loading times. All studies show that nucleation, growth and coalescence of micro-voids and micro-cracks play the most important role in ductile and quasi-brittle spall failure. In general, majority of spall criteria are based on an critical stress. However, among many propositions the criteria which are based on cumulative approach are commonly accepted.

One of the experimental configurations used to study spalling involves impacting a flyer plate against a flat target specimen of the same or different material. The superposition of two waves in the target plate, incident and reflected, sets material in tension and causes local internal damage leading to spalling. A special gas launcher, entirely automated and controlled by computer software, has been developed some years ago in the Laboratory of the Mechanics and Physics of Solids (LPMM). In typical experiment different loading intervals are applied at the same stress level (constant impact velocity) to obtain the incipient spall stress vs. loading time. The results obtained for an armor steel can be presented in the form of spall stress versus loading time, such data are shown in Fig.41, [32]. It is observed in this figure that the spall stress increases when the loading time decreases, which can be interpreted as an evidence of a cumulative process of spall fracturing and rate sensitivity.

Some time ago a new local and cumulative failure criterion, applicable to the tensile mode of loading , has been proposed, [11]. The Boltzmann statistics has been applied for short and very short loading times or relatively low temperatures. The critical time to fracture with the threshold stress σ_F is given by the relation

$$t_c = t_{C0} \exp\left(-\frac{\Delta G(\sigma_F)}{kT}\right) \tag{7}$$

where $\Delta G(\sigma_F)$ is the stress-dependent free energy of activation taken in the form after Yokobori, [33]

$$\Delta G(\sigma_F) = G_0 \ln\left(\frac{\sigma_F}{\sigma_{F0}}\right) \tag{8}$$

where t_{Co} and σ_{Fo} define the characteristic point for the longest critical time, σ_F is the threshold stress for spalling. Thus, the following cumulative fracture criterion in the form of the following integral has been derived

$$t_{Co} = \int_0^{t_c} \left(\frac{\sigma_F(t)}{\sigma_{Fo}} \right)^{\alpha(T)} dt \tag{9}$$

with $\alpha(T) = \Delta G_0 / kT$. Finally, σ_{Fo}, t_{Co} and $\alpha(T)$ are three material constants at constant temperature. When the process is non-isothermal, as it happens locally in the case of spalling, the exponent $\alpha(T)$ is time-dependent via changes of temperature during loading or unloading., then $\alpha(T,t)$. In special cases of square pulse, corresponding to experiments with impact plates, the criterion can be integrated and the adequate relation takes the form

$$\sigma_F = \sigma_{Fo} \left(\frac{t_{Co}}{t_C} \right)^{1/\alpha(T)} \tag{10}$$

As an illustration the criterion constants have been identified for two materials and the result is compared with experimental data in Fig.42. For the first material, which is an aluminum alloy, σ_{Fo} = 1.068 GPa, α = 1.360 and t_{Co}=2.0 μs; for an armor steel, σ_{Fo} = 4.9 GPa, α = 2.369 and t_{Co} = 2.0 μs.

Unfortunately, there is no data to identify all material constants for Ti-6Al-4V. Such a research program could be envisaged in the future.

In order to calculate numerically penetration or perforation processes during impact by FE codes those TWO criteria must be introduced simultaneously. Some results of numerical calculations with the failure criteria in shear have been reported in [1,7,8,23]. They predict correctly the failure processes at different impact velocities.

8. Discussion

The most important factor in the numerical analyses of all problems in impact mechanics are constitutive relations. Many has been proposed so far, however, at

strain rates higher than ~10^E3 1/s a specific behavior emerges, a very high rate sensitivity is combined with adiabatic heating and very low of strain hardening. All those features are taken into consideration in constitutive relations developed in LPMM-Metz; Eqs (1), (2) and (3). Those constitutive relations are suffciently simple and flexible to be applied in numerical codes. Identification of constants can be optimized by a special procedure.

In the previous Report some numerical simulations of the standard MDS specimen were presented for Ti-6Al-4V, [1]. The study of the existing stress concentrators, and theirs role as a trigger of adiabatic failure was one of the objectives of those numerical analyses. The final results obtained with the ABAQUS explicit FE code, [7,8,22,23], confirm existence of the Critical Impact Velocity (CIV) in shear. The estimated value of CIV from FE calculations was $V_C = 132$ m/s and the theoretical analysis, [4,5,8], yielded close value of $V_C = 121$ m/s.

The CIV in shear is a new material constant which can characterize materials in respect to fragmentation and perforation. Thus, the CIV in shear has a far reaching consequences in fragmentation and perforation. Experiments performed with MDS specimens (standard geometry) made of Ti-6Al-4V alloy clearly indicate on a decrease of the fracturing energy when the impact velocity exceeded ~100 m/s. The estimation of energy to failure by the FE method as a function of the impact velocity leads to the conclusion that above CIV a considerable decrease of failure energy occurs, that is for the impact velocity $V_i = 100$ m/s and higher [1,8].

It has been found that the local failure criterion based on adiabatic process of plastic deformation is rate-dependent, Fig.39 and Fig.40. Application of such criterion in FE code ABAQUS yields good results as compared to experimental data. It has been confirmed previously that the local failure criterion based on the strain energy density, comparison given in Fig.39, is similar to the failure strain criterion.

Experimental failure shear stress is almost the same for all three stress concentrators, "U", "V" and "I", at different nominal strain rates, Fig. 23 for example. The energy analysis, Fig.28 to Fig.33, clearly confirms superiority of the local failure criteria based on the effective strain in 3D cases or on the strain energy density. The local failure criteria should be also verified numerically for three different specimen geometries applied in experiments, but such a program exceeds the tasks of this research.

In a complete FE applications a failure criterion for spalling must be also applied at the same time. The criterion for spalling discussed in the previous part of this Report is a cumulative one and it has been applied so far in numerical codes for practical problems, [34, GIAT-private communication].

Comparison of the critical shear strains to failure for VAR 4340 steel and Ti-6Al-4V indicates that at high local shear strain rates the steel behaves in a much "brittle" manner than the titanium alloy. Simply, concerning ASB the carrying capacity of the titanium alloy is locally much higher than VAR 4340 steel ~52 HRC, [36,37]. Of course, behavior of steels depends on the level of hardness [36].

Experimental Technique based on DS concept assures a reliable tool to test materials in shear within a very wide range of strain rates. Application of specimens with different stress concentrators can be very helpful in numerical studies of local failure criteria in adiabatic conditions of deformation. In general, a hybrid method (experiment plus FE verification) or inverse techniques are extremely useful in development of local failure criteria in shear and in tension.

9. Final Conclusions

The main conclusions after the research program reported above can be drawn.

1) Experimental techniques of Double Shear (DS) has been perfected, it has been applied to perform a series of tests at different impact velocity with three stress concentrators: "U", "V" and "I".
2) All digital records were analyzed to obtain nominal shear stress vs. nominal shear strain characteristics at different nominal strain rates (impact velocities). In total more than 60 tests have been performed.
3) The tests at high nominal strain rates have shown a very high rate sensitivity of Ti-6Al-4V alloy. But at the nominal strain rates higher than $2*10^{E}4$ 1/s the stress concentrators begin to dominate.
4) Experimental data obtained for the standard specimen geometry were used to identify all material constants in an unique constitutive relations applicable to FE codes
5) Two failure criteria have been discussed, that is for adiabatic shear and spalling. The criterion based on the failure strain has been completely identified. The spall criterion lacks of constant identification. New

experiments with the plate-plate technique should be performed for Ti-6Al-4V.

6) The critical impact velocity (CIV) in shear has been analyzed for Ti-6Al-4V.

The study was to focussed on finding the resistance of Ti-6Al-4V alloy to formation of Adiabatic Shear Bands (ASB) and failure at different impact velocities including the range of velocities up to 100 m/s (nominal shear strain rate $5*10^{E}5$).

A clear picture emerges from the scenarios given above. All effects under discussion , that is the ability to strain hardening, rate- and temperature sensitivities, adiabatic increase of temperature, stress concentrators and the CIV in shear, play an important role in resistance to impact loading and fragmentation. The thermal treatment and the final microstructure are the key factors in the optimization process. Further studies should be focussed on hybrid techniques (experiment and FE codes) with a complete identification of failure criteria.

Acknowledgements

The research reported herein was sponsored in part by the US Army trough its European Research Office, Contract N° : N68171-98-M-5829, and in part by CNRS-France. Acknowledgement are also due to Dr. W.A.Gooch of ARO - USA for fruitful discussions.

References

[1] J.R.Klepaczko, Effects of impact velocity and stress concentrators in titanium on failure by adiabatic shearing, Final Technical Report for US Army European Res. Office, Contract N68171-98-M-5829, LPMM, Metz University, (1999).

[2] J.R.Klepaczko, An experimental technique for shear testing at high and very high strain rates. The case of a mild steel, Int. J. Impact Engng., **15** (1994), pp. 25-39.

[3] J.R.Klepaczko, Experimental Investigation of Adiabatic Shear Banding at Different Impact Velocities, Final Technical Report for the US Army European Res. Office, Contract DAJA 49-90-C-0052, LPMM, Metz University, (1993).

[4] J.R.Klepaczko, Plastic shearing at high and very high strain rates, Proc. Int. Conf. EURODYMAT 94, J. de Physique IV, Coll. C8, **4** (1994), pp.C8-35 - C8 -40.

[5] J.R.Klepaczko, On the critical impact velocity in plastic shearing, Proc. of Int. Conf. EXPLOMET'95, Elsevier Science, (1995), 413.

[6] M.Klosak and J.R.Klepaczko, Numerical study of the Critical Impact Velocity in Shear, Appendix N° 1, Final Technical Report prepared for the US Army European Res. Office, Contract DAJA N68171-95-C-9071, LPMM, Metz University (1996).

[7] J.R.Klepaczko and M. Klosak, Numerical study of the critical impact velocity in shear, Eur. J. Mech., A/Solids, **18** (1999), 93.

[8] A.S.Lebouvier and J.R.Klepaczko, Numerical study of fast shearing and the critical impact velocity in shear, case of Ti-6Al-4V, Int. J. Impact Engng, (2001), submitted.

[9] Y.Me-Bar and Z.Rosenberg, On the Correlation Between the Ballistic Behavior and Dynamic Properties of Titanium-alloy Plates, Int. J. Impact Engng. , **19** (1997), pp. 311-318.

[10] L.W.Meyer, L.Krueger, W.A.Gooch and M.S.Burkins, Analysis of Shear Band Effects in Titanium Relative to High Strain-rate Laboratory/Ballistic Impact Tests, Proc. Int. Conf. EURODYMAT 97, J.de Physique IV, (1997), pp.

[11] J.R.Klepaczko, Dynamic crack initiation, some experimental methods and modeling, in : Crack Dynamics in Metallic Materials, Springer Verlag, Wienna - NY (1990).

[12] I.V.Varfolomeyev and J.R.Klepaczko, Approximate Analysis on Strain Rate Effects and Behavior of Stress and Strain Fields at Crack Tip in Mode II in Metallic Materials, Appendix N° 1 to the Technical Report for the US Army European Res. Office, Contract DAJA 45-90-C-0052, LPMM, Metz University (1992).

[13] I.V. Varfolomayer and J. R. Klepaczko, Approximate analysis of strain rate effects and behavior of stress and strain fiels at the crack tip in Mode II in metallic materials, Strengh of Materials (Problems Prochnosti), N° 3, (1995), 46.

[14] J.R.Klepaczko, P. Lipinski and A. Molinari, An analysis of the thermoplastic catastrophic shear in some metals, in : Impact Loading and Dynamic Behavior of Materials, DGM Informationsgesellschaft Verlag, Oberursel, Vol. 2, (1988),

[15] J.R.Klepaczko and B.Rezaig, A numerical study of adiabatic shear banding in mild steel by dislocation mechanics based constitutive relations, Mech. of Materials, **24** (1996), 125.

[16] J.R. Klepaczko, Experimental Investigation of Adiabatic Shear Banding at Different Impact Velocities, Final Technical Report for the ERO of the US Army, Contract N°DAJA45-90-C-0052, LPMM-Metz University, (1993).

[17] T.Kàrmàn and P.E.Duvez, The propagation of plastic deformation in solids, J. Appl. Phys., **21** (1950), pp. 987-994.

[18] J.R.Klepaczko, Generalized conditions for stability in tension test, Int. J. Mech. Sci., **10** (1968), pp.297-313.

[19] D.C.Erlich, D.R.Curran and L.Seaman, Further Development of a Computational Shear Band Model, Report AMMRC TR80-3, SRI International (1980).

[20] J.W.Swegle and D.B.Grady, Calculation of thermal trapping in shear bands, in: Metallurgical Application of Shock-Wave and High-Strain Rate Phenomena, Marcel Dekker, Inc., N.Y. (1986), pp. 705-722.

[21] F. H. Wu and L. B. Freund, Deformation trapping due to thermoplastic instability in one-dimensional wave propagation, J. Mech. Phys. Solids, **32** (1984), 119

[22] J.R.Klepaczko, Stress Concentrators and Rate Effects in Formation of Adiabatic Shear Bands, Technical Report for the US Army European Res. Office, Contract N68171-95-C-9071, LPMM, Metz University (1996).

[23] J.R.Klepaczko, Stress Concentrators and Rate Effects in Formation of Adiabatic Shear Bands, Technical Report for the European Res. Office of the US Army, Contract N°: N68171-97-C-9003, (1998).

[24] Martin G.H.Wells, The Mechanical and Ballistic Properties of an Electron Beam Single Melt of Ti-6Al-4V Plate, AMSRL-WM-MC, (Sept. 1998).

[25] ABAQUS Manual, Version 5.8, Hbbit, Karlsson and Sorensen, Inc., Providence, RI, USA (2000)

[26] J.R.Klepaczko, A pratical stress-strain strain-rate temperature constitutive relation of the power from, J. Mech. Working Technology, **15** (1987),143.

[27] J.R.Klepaczko, Modeling of microstructural evolution at medium and high strain rates, FCC and BCC metals, in Constitutive Relations and Their Physical Basis, Riso Natl. Laboratory, Roskilde, Danemark (1987), 387.

[28] J.R.Klepaczko, A general approach to rate sensitivity and constitutive modeling of FCC metals, in Impact: Effects of Fast Transient Loadings, A.A.Balkema, Rotterdam, (1988), 3.

[29] P.Chwalik, Numerical Analysis and Constitutive Relation of TA6V, DEA Report, LPMM, Metz University, (2000).

[30] J.Hodowany, G.Ravichandran and A.J.Rosakis, On the strain and strain rate dependence of the fraction of plastic work converted to heat: an experimental study using high speed infrared detectors and the Kolsky bar, Tech. Rep. California Inst. of Technology, Pasadena (1997).

[31] J.R.Klepaczko, Recent progress in testing of materials in impact shearing , Proc.of the 1995 Joint ASME/JSME Pressure Vessels and Piping Conf. PVP -Vol.300, Dynamic Fracture, Failure, and Deformation, ASME (1995), 165..

[32] P.Chevrier and J.R.Klepaczko, Spall fracture: Mechanical and microstructural aspects, Eng. Fracture Mech., **63** (1999) , 273.

[33] T.Yokobori, The Cottrell-Bilby theory of yielding in iron, J.Appl.Phys. (Letters) **23** (1952), 1423.

[34] S.Hanim and J.R.Klepaczko, Numerical study of spalling in an aluminum alloy 7020-T6, Int. J. Impact Eng., **22** (1999), 649.

[35] L.W.Meyer, L.Krueger, W.A.Gooch and M.S.Burkins, Analysis of shear band effects in titanium relative to high strain-rate laboratory/ballistic impact tests, Proc. Int. Conf. EURODYMAT 97, J.de Physique IV, (preprint).

[36] Y. C. Chi, S. Lee, K. Cho and J. Dufty, The effects to tempering and test

temperature on the dynamic fracture initiation behavior of an AISI 4340 VAR steel, Mat. Sci. and Engng., **A114** (1989), 105.

[37] J. G. Cowie, The Influence of second-phase dispersions on shear instability and fracture toughness of ultrahigh strengh 4340 steel, Report N° MTL TR 89-20, US Army Materials Technology Laboratory, Watertown, MA (March 1989).

TABLES

FIGURE CAPTIONS

Fig. 1 Configuration of experimental setup for impact shearing of the MDS specimen and specimens with stress concentrators..

Fig. 2 Modified Double Shear (MDS) specimen, standard geometry.

Fig. 3 Specimen dimensions for "U", "V" and "I" geometry.

Fig. 4 Proof Stress and Tensile Strength as a function of temperature for Ti-6Al-4V , grade 5.

Fig. 5 Elongation over gage length 50 mm as a function of temperature for Ti-6Al-4V, grade 5.

Fig. 6 Digital record of DS test on MDS specimen with experimental setup shown in Fig.1; standard geometry, V = 19.0 m/s.

Fig. 7 Digital record of DS test on MDS specimen with experimental setup shown In Fig.1; standard geometry, V = 24.5 m/s.

Fig. 8 Device for quasi-static loading of DS specimens, 1-base support, 2-specimen support, 3-DS specimen, 4-punch, 5-LVDT displacement gage, 6-independent load cell.

Fig. 9 Typical record of "quasi-static" shear test, servo-hydraulic machine.

Fig.10 Results of quasi-static tests on "U", "V" and "I" specimens. Maximum nominal shear stress vs. logarithm of strain rate, Ti-6Al-4V.

Fig.11 Record of direct impact test, "U" geometry, impact velocity V = 52.34 m/s.

Fig.12 Record of direct impact test, "U" geometry, impact velocity V = 88.51 m/s.

Fig.13 Record of direct impact test, "V" geometry, impact velocity V = 42.81 m/s.

Fig.14 Record of direct impact test, "V" geometry, impact velocity V = 81.99 m/s.

Fig.15 Record of direct impact test, "I" geometry, impact velocity V = 41.99 m/s.

Fig.16 Record of direct impact test, "I" geometry, impact velocity V = 78.74 m/s.

Fig.17 Direct impact tests, "U" geometry, maximum shear stress vs. impact velocity.

Fig.18 Direct impact tests, "V" geometry, maximum shear stress vs. impact velocity.

Fig.19 Direct impact tests, "I" geometry, maximum shear stress vs. impact velocity.

Fig.20 Strain rate spectrum for "U" geometry, maximum shear stress vs. logarithm of strain rate.

Fig.21 Strain rate spectrum for "V" geometry, maximum shear stress vs. logarithm of strain rate.

Fig.22 Strain rate spectrum for "I" geometry, maximum shear stress vs. logarithm of strain rate.

Fig.23 Comparison of the strain rate spectra for "U", "V" and "I" geometry, maximum shear stress vs. logarithm of strain rate.

Fig.24 Stages of shear stress vs. shear strain during fast shearing in adiabatic Conditions, black points indicates failure.

Fig.25 Schematic evolution of shear stress vs. shear strain for increasing strain rates, 1- the lowest strain rate (order 10^E2 1/s), 4-the highest strain rate (order 10^E5 1/s).

Fig.26 Energy at maximum stress, "U", "V" and "I" profiles, vs. logarithm of strain rate, quasi-static range of strain rates.

Fig.27 Energy at maximum stress, "U", "V" and "I" profiles, vs. logarithm of strain rate, direct impact tests.

Fig.28 Energy at failure (total energy), "U", "V" and "I" profiles, vs. logarithm of strain rate, quasi-static range of strain rates.

Fig.29 Energy at failure (total energy), "U", "V" and "I" profiles, vs. impact velocity, direct impact tests.

Fig.30 Energy at maximum stress, "U", "V" and "I" profiles, vs. logarithm of strain rate, entire rate spectrum.

Fig.31 Energy at failure (total energy), "U", "V" and "I" profiles, vs. logarithm of strain rate, entire rate spectrum.

Fig.32 Mean values of failure energy for VAR 4340 steel for "S", "U", "V" and "I" geometry, vs. logarithm of strain rate, "S"-standard geometry.

Fig.33 Failure energy vs. impact velocity, results of FE simulation for VAR 4340 steel, "S", "U", "V" and "I" geometry.

Fig.34 Contour of broken MDS specimen (standard geometry), broken lines indicate shear strain at maximum stress (instability shear strain).

Fig.35 Shear strain of instability determined by the contour measurements vs. logarithm of strain rate, direct impact tests on "S" specimens.

Fig.36 Instability shear strain determined by the contour measurements compared with constitutive model prediction for Ti-6Al-4V.

Fig.37 Mean values of the nominal shear strain Γ_m at maximum stress for VAR 4340 steel, "S", "U", "V" and "I" geometry, vs. logarithm of strain rate.

Fig.38 Mean values of the nominal shear strain Γ_C at failure for VAR 4340 steel "S", "U", "V" and "I" geometry, vs. logarithm of the nominal strain rate.

Fig.39 Local failure criteria for VAR 4340 steel. Predicted values of the failure local strain Γ_C and the critical energy density vs. logarithm of strain rate.

Fig.40 Local failure shear strain Γ_C for Ti-6Al-4V as estimated by inverse method vs. logarithm of strain rate.

Fig.41 Incipient spall stress vs. loading time for an armor steel, [32].

Fig.42 Comparison of the incipient stress for spalling for two materials: armor steel and aluminum alloy, experimental points compared with spall criterion - -solid lines, Eq.(9).

Files			Nominal strain rate (s^{-1})
Profile U	**Profile V**	**Profile I**	
TUHA01	TVHA02	TIHA01	0.001
TUHA02	TVHA03	TIHA02	0.001
TUHA03	TVHA04	TIHA03	0.01
TUHA04	TVHA05	TIHA04	0.01
TUHA05	TVHA06	TIHA05	0.1
TUHA06	TVHA07	TIHA06	0.1
TUHA07	TVHA08	TIHA07	1
TUHA08	TVHA09	TIHA08	1
TUHA09	TVHA10	TIHA09	10
TUHA10	TVHA11	TIHA10	10
TUHA11	TVHA12	TIHA11	100
TUHA12	TVHA13	TIHA12	100
TUHA13			100
TUHA14			10

Table 1

Files	Nominal strain rate (s^{-1})	Impact velocity (ms^{-1})
TUHA15	6200	12.4
TUHA16	8500	17
TUHA18	13630	27.26
TUHA19	13845	27.69
TUHA20	28810	57.62
TUHA21	26170	52.34
TUHA22	34530	69.06
TUHA23	34805	69.61
TUHA24	38915	77.83
TUHA25	38775	77.55
TUHA26	11640	23.28
TUHA27b	12620	25.24
TUHA28	10105	20.21
TUHA29	10070	20.14
TUHA30	20720	41.44
TUHA31	21320	42.64
TUHA32	11590	23.18
TUHA33	44250	88.5
TUHA34	11055	22.11

Table 2

Files	Nominal strain rate (s^{-1})	Impact velocity (ms^{-1})
TVHA14	8430	16.86
TVHA16	12440	24.88
TVHA17	14045	28.09
TVHA18	15220	30.44
TVHA19	17145	34.29
TVHA20	25965	51.93
TVHA21	34820	69.64
TVHA22	34860	69.72
TVHA23	40995	81.99
TVHA24	39105	78.21
TVHA25b	10230	20.46
TVHA26	9830	19.66
TVHA27	10045	20.09
TVHA28	20580	41.16
TVHA29	21405	42.81
TVHA30	11100	22.2
TVHA31	41050	82.1
TVHA32	44935	89.87
TVHA33	10825	21.65

Table 3

Files	Nominal strain rate (s^{-1})	Impact velocity (ms^{-1})
TIHA13	12640	25.28
TIHA14	8555	17.11
TIHA15	14400	28.8
TIHA16	15490	30.98
TIHA17	27870	55.74
TIHA18	28845	57.69
TIHA19	34650	69.3
TIHA21	39370	78.74
TIHA22	39800	79.6
TIHA23	9995	19.99
TIHA24	10115	20.23
TIHA25	24200	48.4
TIHA26	22400	44.8
TIHA27	20995	41.99
TIHA28b	9645	19.29
TIHA29	37975	75.95
TIHA30	42170	84.34
TIHA31	41350	82.7
TIHA32	10950	21.9

Table 4

paramètres	valeurs	unités
B	815	MPa
ν	1.113	-
Γ_0	$1.6\text{x}10^{-3}$	-
τ_0	750	MPa
D	4 347	K
$\dot{\Gamma}_0$	10^6	s^{-1}
m	0.4	-
μ_0	43.91	GPa
A	$6.808\text{x}10^{-4}$	K^{-1}
C	$1.036\text{x}10^{-7}$	K^{-2}
n_0	0.06	-
T_f	1 900	K
T_0	1	K

Table 5

$$\beta = \beta_0 - a\log\left(\frac{\dot{\Gamma}_0}{\dot{\Gamma}}\right)$$

paramètres	valeurs	unités
β_0	0.9088	-
a	0.0431	-
ρ	4.51	$g.cm^{-3}$
C_v	543	$J.kg.K^{-1}$
T_m	1 900	K

Table 6

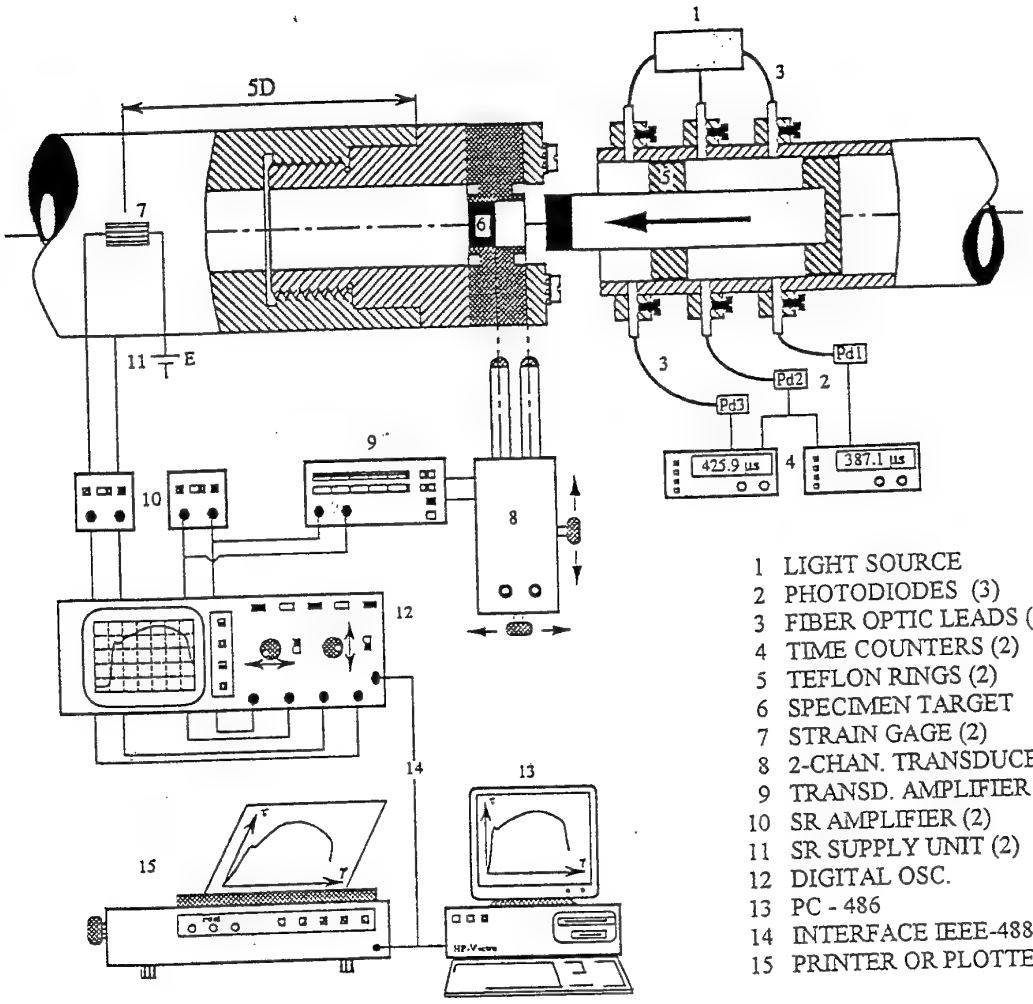

1 LIGHT SOURCE
2 PHOTODIODES (3)
3 FIBER OPTIC LEADS (6)
4 TIME COUNTERS (2)
5 TEFLON RINGS (2)
6 SPECIMEN TARGET
7 STRAIN GAGE (2)
8 2-CHAN. TRANSDUCER
9 TRANSD. AMPLIFIER
10 SR AMPLIFIER (2)
11 SR SUPPLY UNIT (2)
12 DIGITAL OSC.
13 PC - 486
14 INTERFACE IEEE-488
15 PRINTER OR PLOTTER

Fig. 1

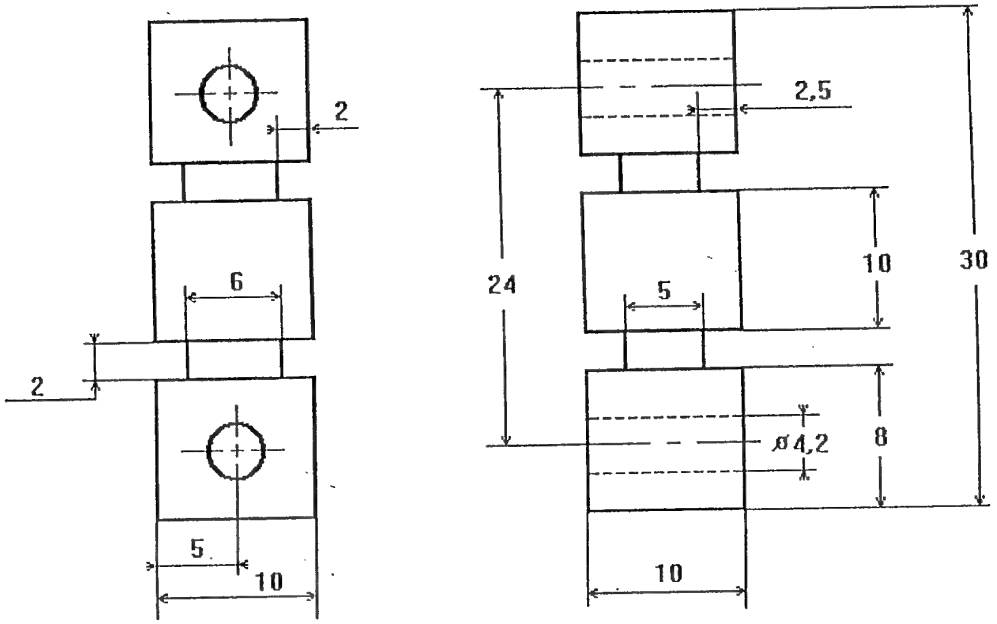

Eprouvettes de double cisaillement
type 1

Fig. 2

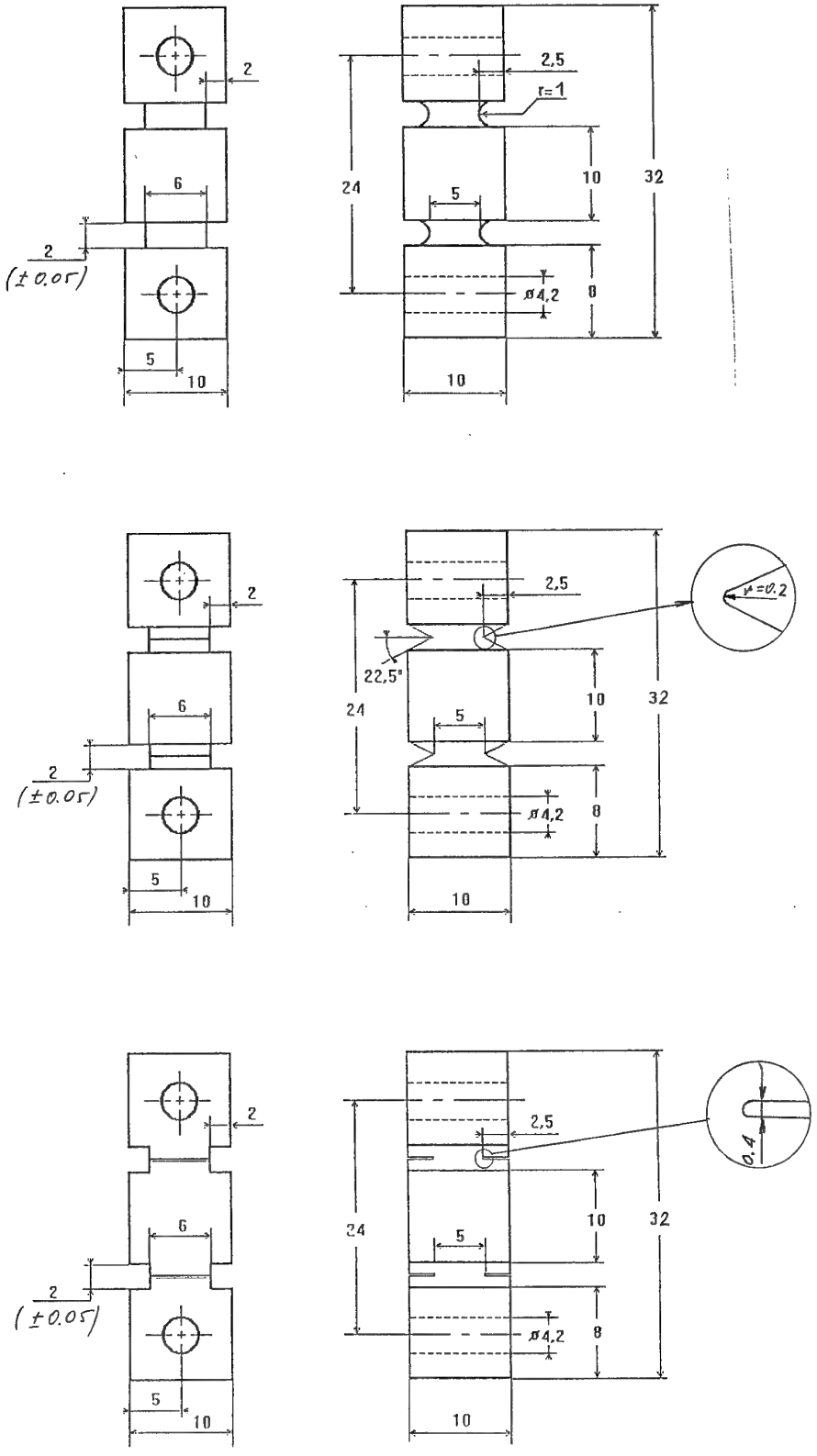

Fig. 3

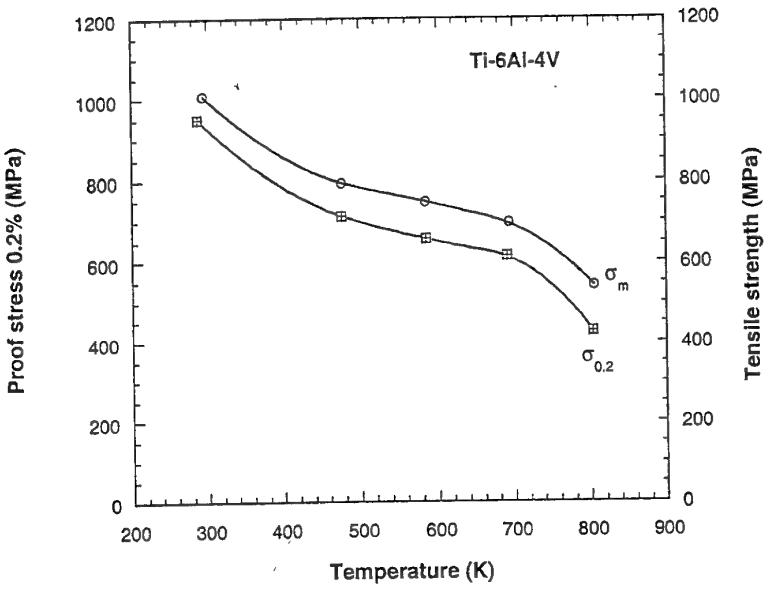
Ti-6Al-4V
Proof stress 0.2% (MPa)
Tensile strength (MPa)
Temperature (K)
σ_m
$\sigma_{0.2}$
0
200
400
600
800
1000
1200
200
300
400
500
600
700
800
900

Fig. 4

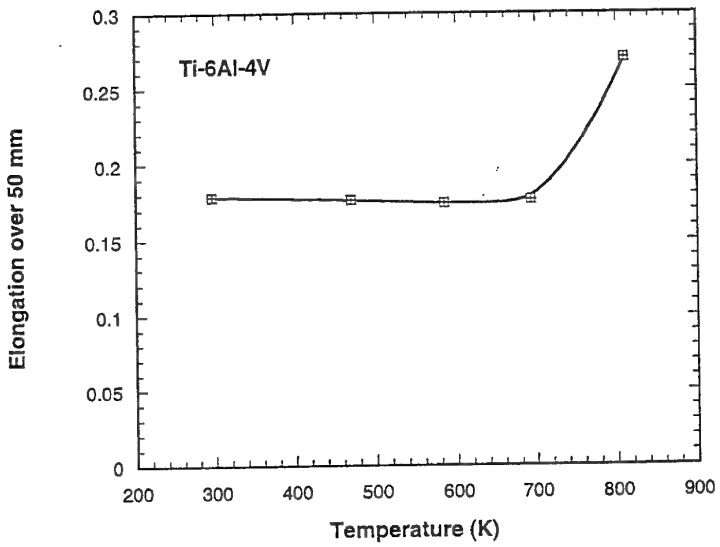
Ti-6Al-4V
Elongation over 50 mm
Temperature (K)
0
0.05
0.1
0.15
0.2
0.25
0.3
200
300
400
500
600
700
800
900

Fig. 5

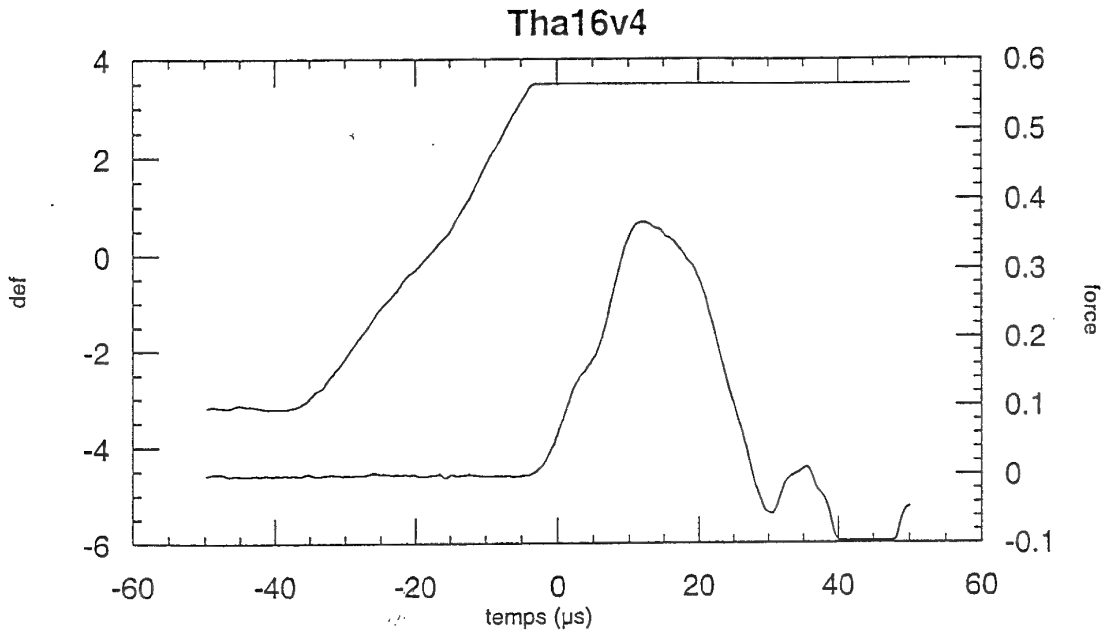
Tha16v4
def
force
temps (µs)
4
2
0
-2
-4
-6
0.6
0.5
0.4
0.3
0.2
0.1
0
-0.1
-60
-40
-20
0
20
40
60

Fig. 6

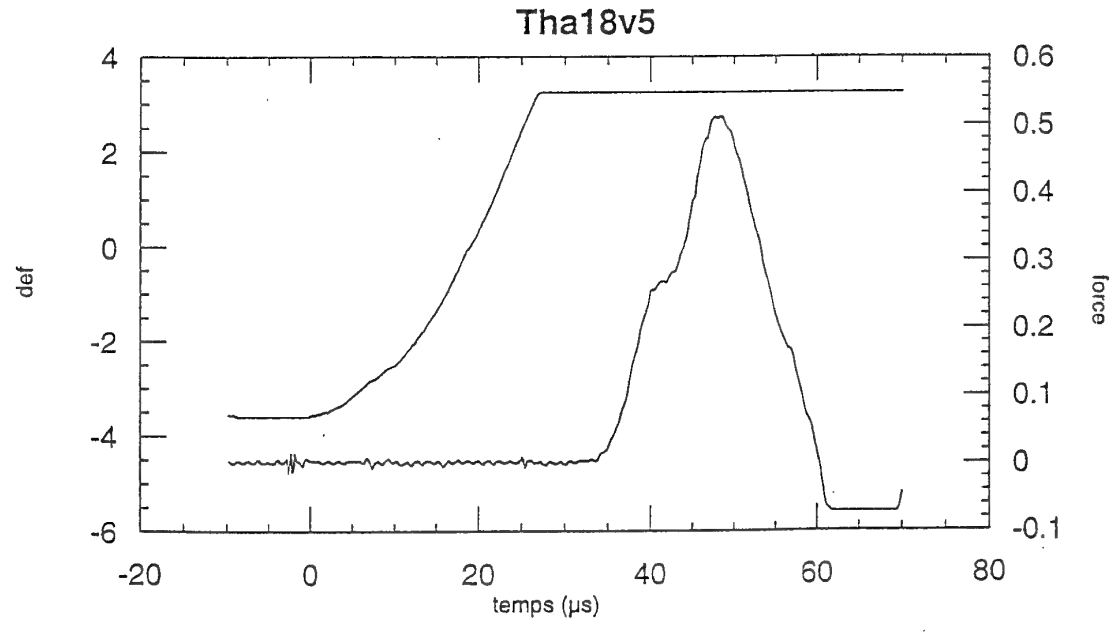
Tha18v5
def
force
temps (µs)
4
2
0
-2
-4
-6
0.6
0.5
0.4
0.3
0.2
0.1
0
-0.1
-20
0
20
40
60
80

Fig. 7

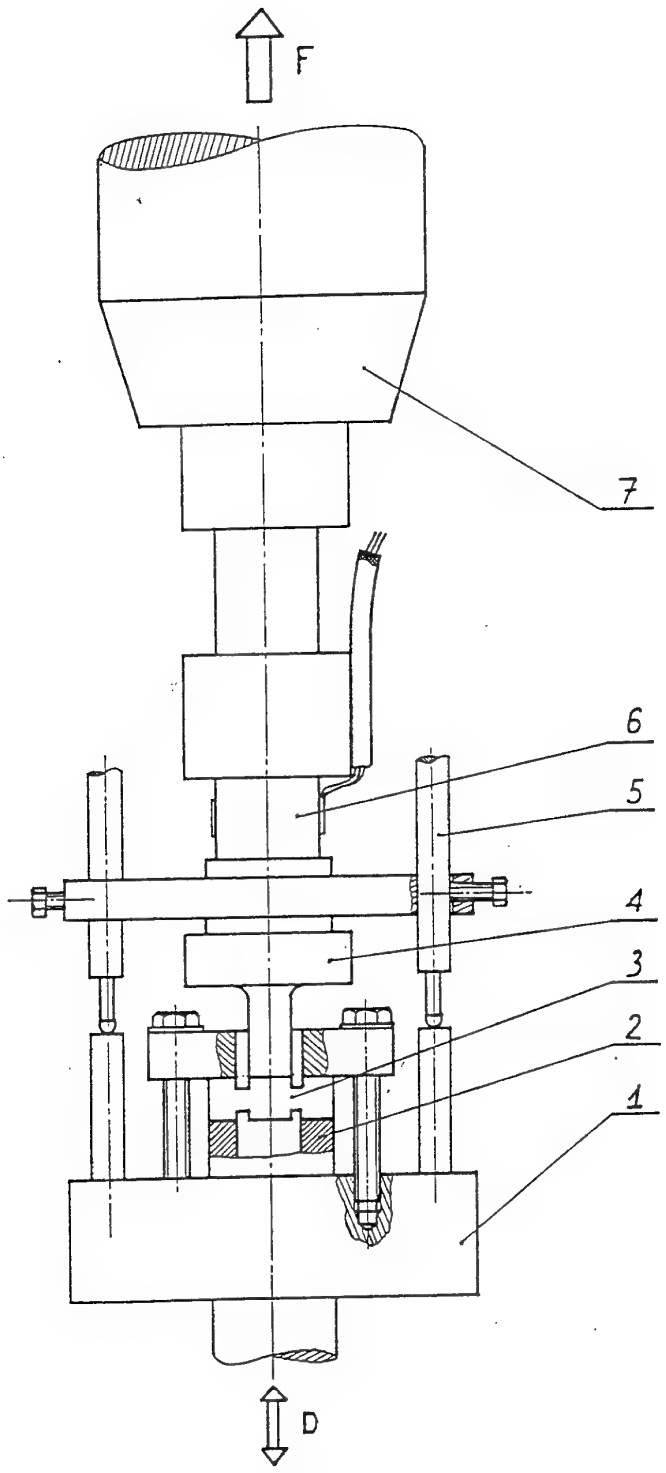

Fig. 8

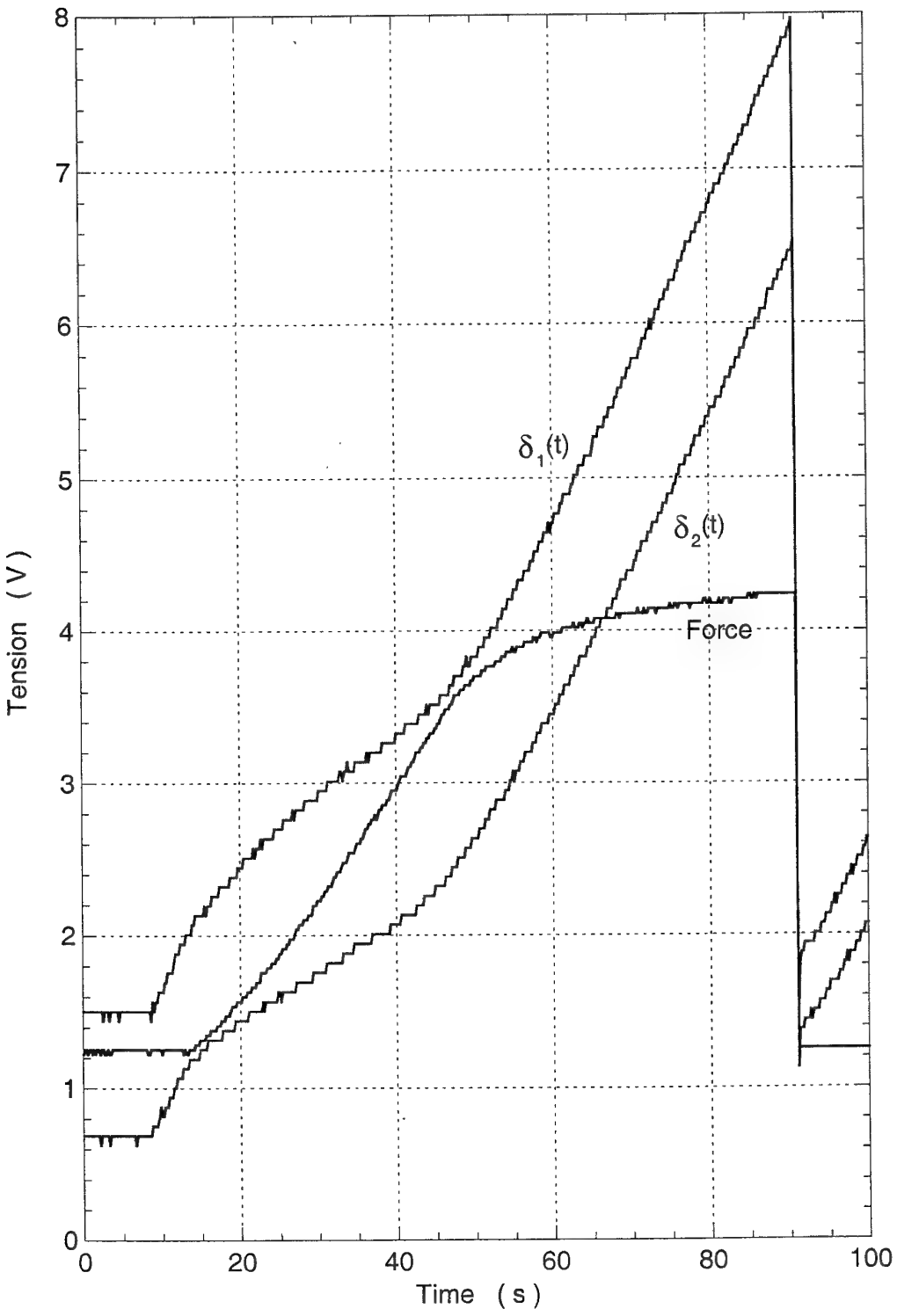
TU04V2
Tension (V)
Time (s)
$\delta_1(t)$
$\delta_2(t)$
Force
0
1
2
3
4
5
6
7
8
0
20
40
60
80
100

Fig. 9

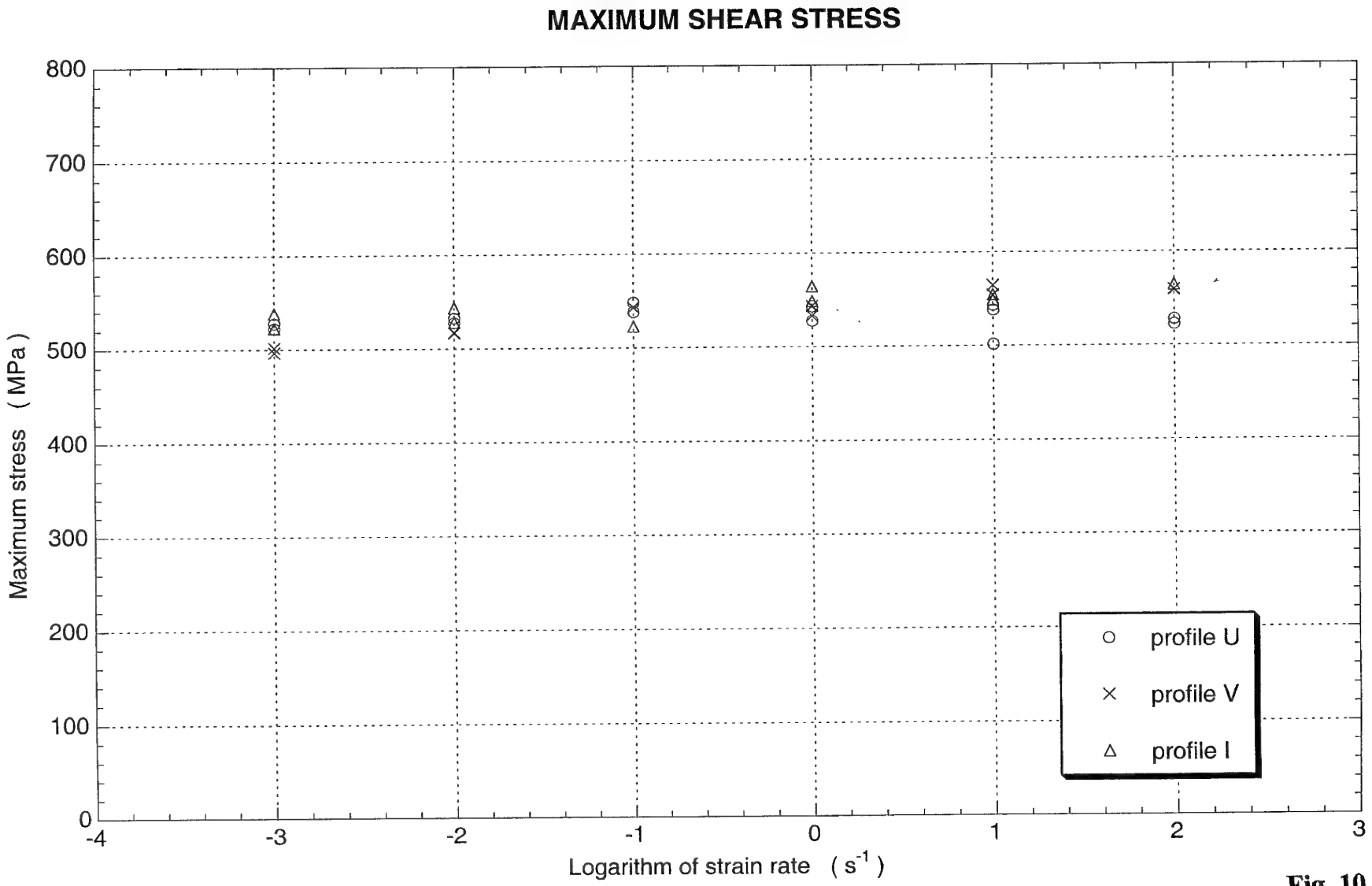
MAXIMUM SHEAR STRESS
800
700
600
500
400
300
200
100
0
Maximum stress (MPa)
-4
-3
-2
-1
0
1
2
3
Logarithm of strain rate (s-1)
profile U
profile V
profile I

Fig. 10

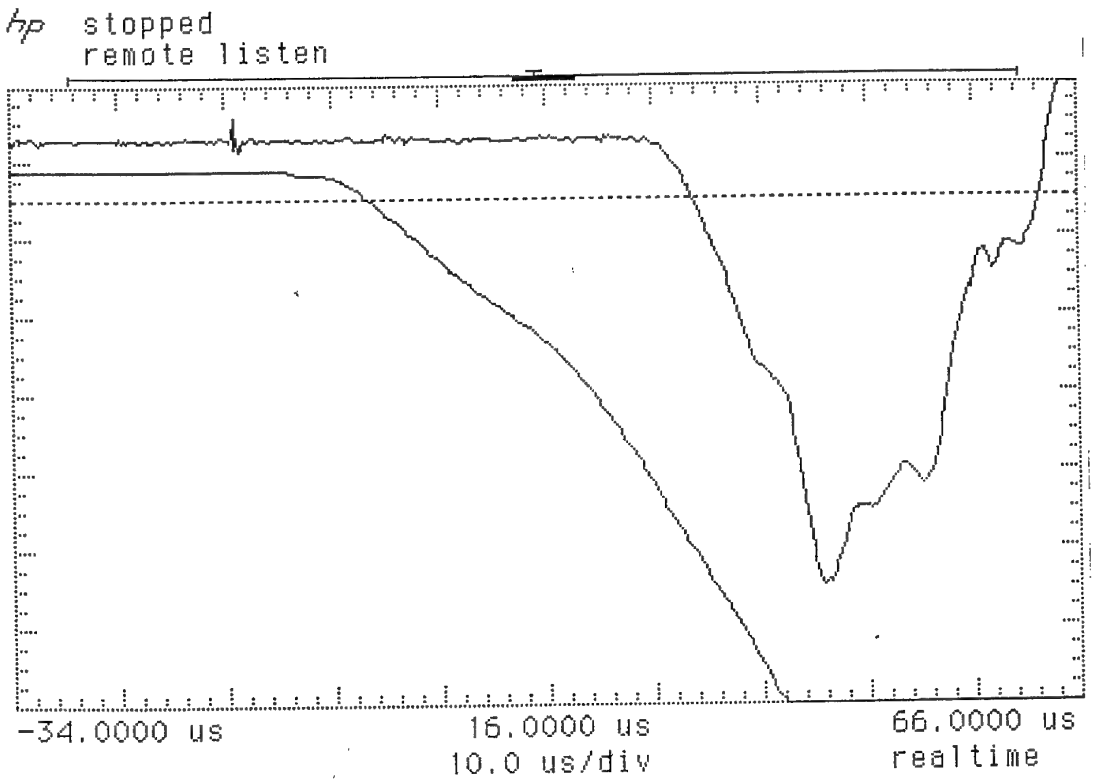
hp stopped
remote listen
-34.0000 us
16.0000 us
10.0 us/div
66.0000 us
realtime

Fig. 11

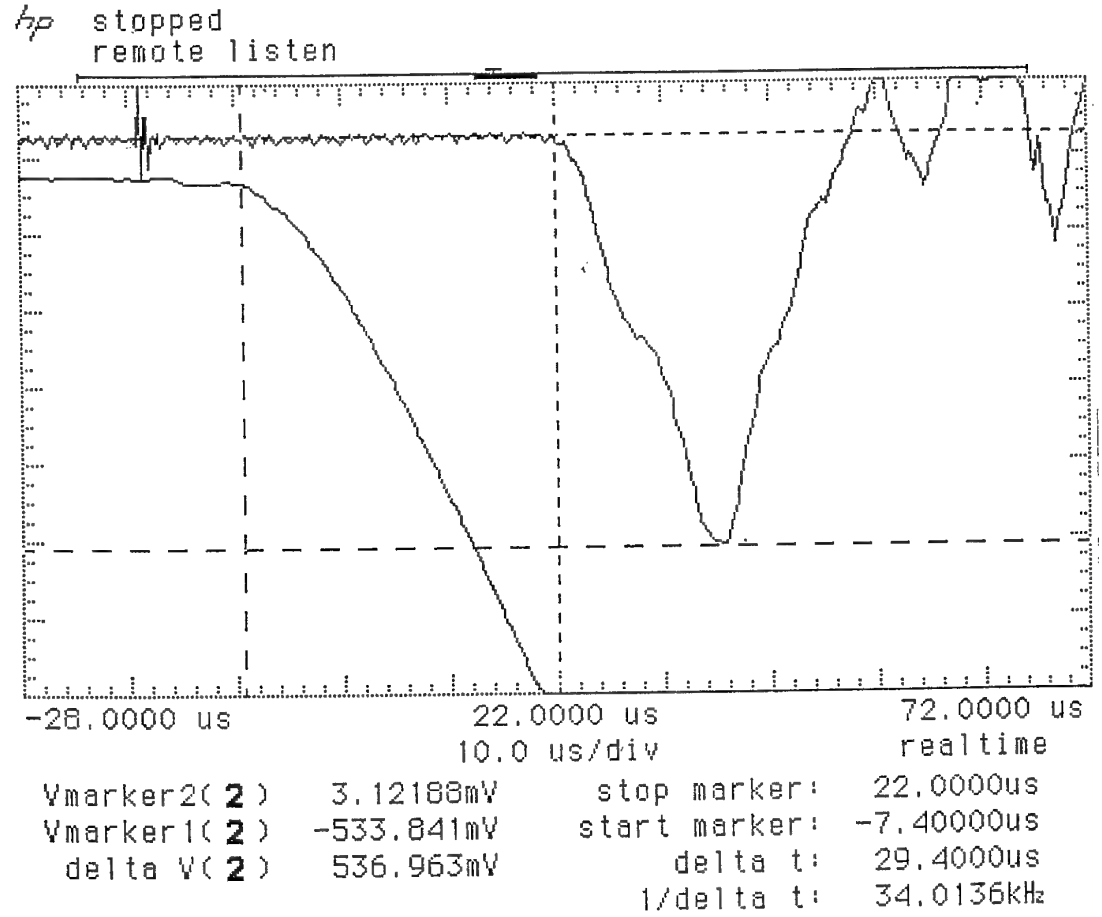
hp stopped
remote listen
-28.0000 us
22.0000 us
10.0 us/div
72.0000 us
realtime
Vmarker2(2) 3.12188mV
Vmarker1(2) -533.841mV
delta V(2) 536.963mV
stop marker: 22.0000us
start marker: -7.40000us
delta t: 29.4000us
1/delta t: 34.0136kHz

Fig. 12

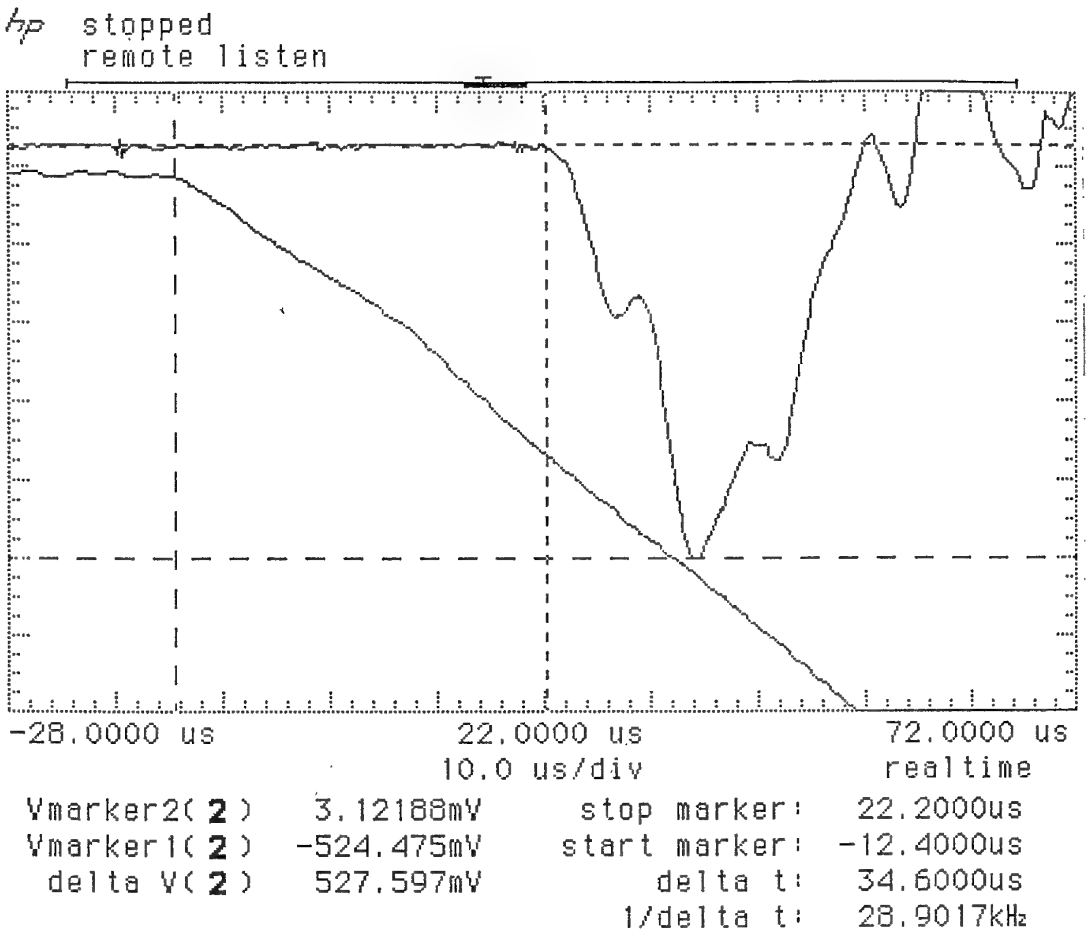
hp stopped
remote listen
-28.0000 us
22.0000 us
10.0 us/div
72.0000 us
realtime
Vmarker2(2) 3.12188mV
Vmarker1(2) -524.475mV
delta V(2) 527.597mV
stop marker: 22.2000us
start marker: -12.4000us
delta t: 34.6000us
1/delta t: 28.9017kHz

Fig. 13

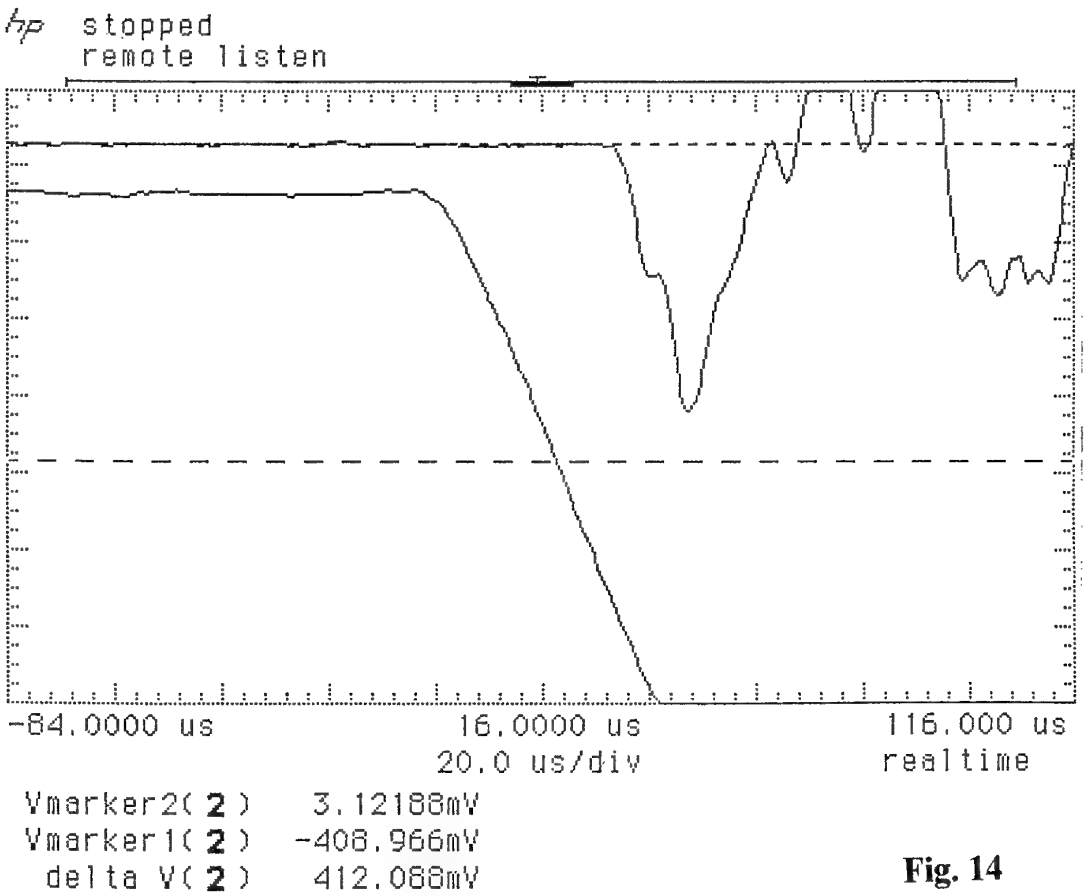
hp stopped
remote listen
-84.0000 us
16.0000 us
20.0 us/div
116.000 us
realtime
Vmarker2(2) 3.12188mV
Vmarker1(2) -408.966mV
delta V(2) 412.088mV

Fig. 14

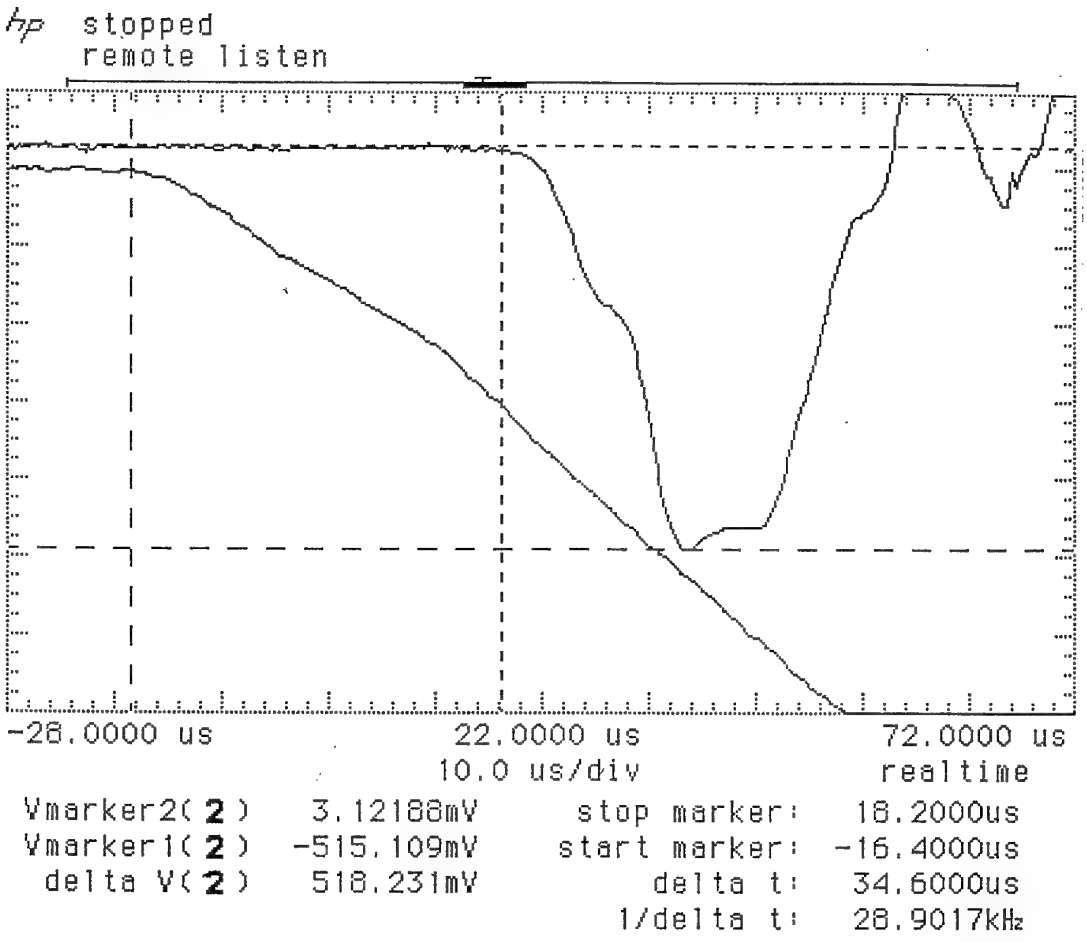
stopped
remote listen
-26.0000 us
22.0000 us
10.0 us/div
72.0000 us
realtime
Vmarker2(2) 3.12188mV
Vmarker1(2) -515.109mV
delta V(2) 518.231mV
stop marker: 18.2000us
start marker: -16.4000us
delta t: 34.6000us
1/delta t: 28.9017kHz

Fig. 15

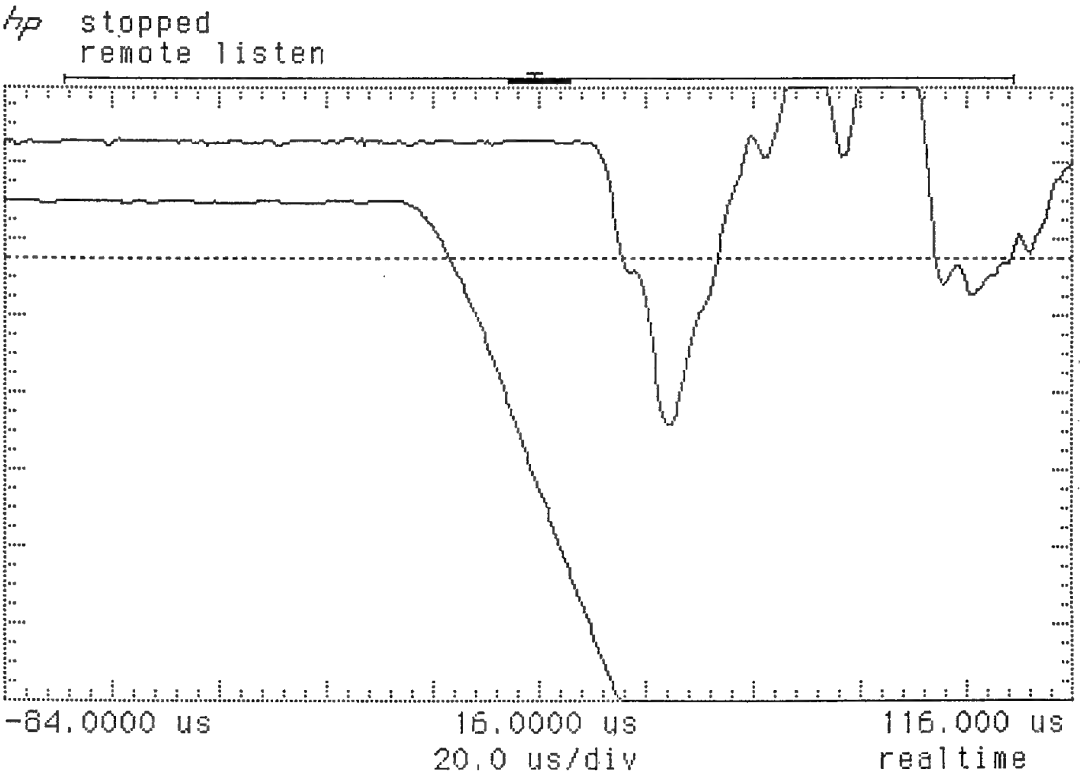
stopped
remote listen
-84.0000 us
16.0000 us
20.0 us/div
116.000 us
realtime

Fig. 16

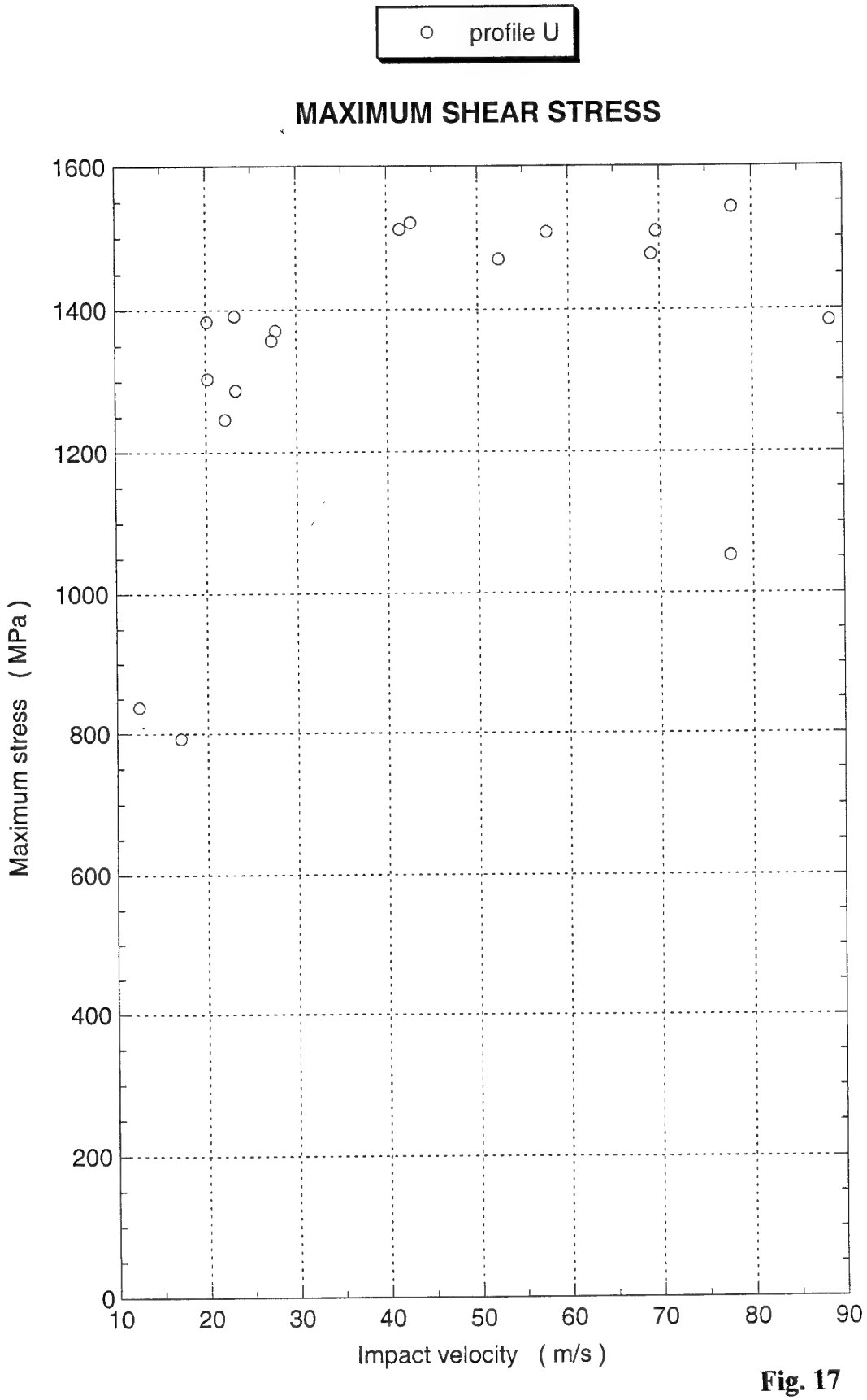
profile U
MAXIMUM SHEAR STRESS
Maximum stress (MPa)
Impact velocity (m/s)
0
200
400
600
800
1000
1200
1400
1600
10
20
30
40
50
60
70
80
90

Fig. 17

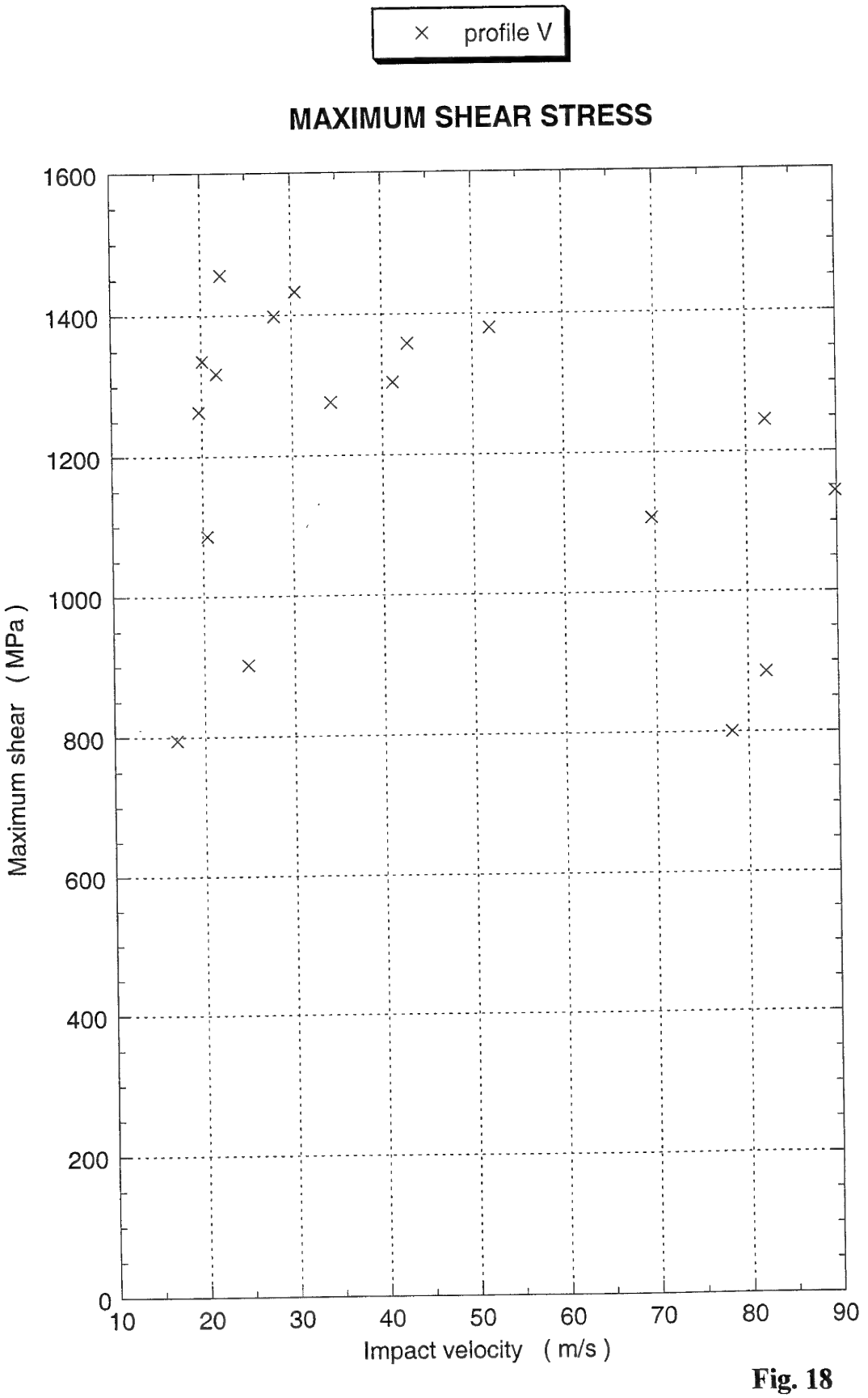
× profile V
MAXIMUM SHEAR STRESS
Maximum shear (MPa)
1600
1400
1200
1000
800
600
400
200
0
10
20
30
40
50
60
70
80
90
Impact velocity (m/s)

Fig. 18

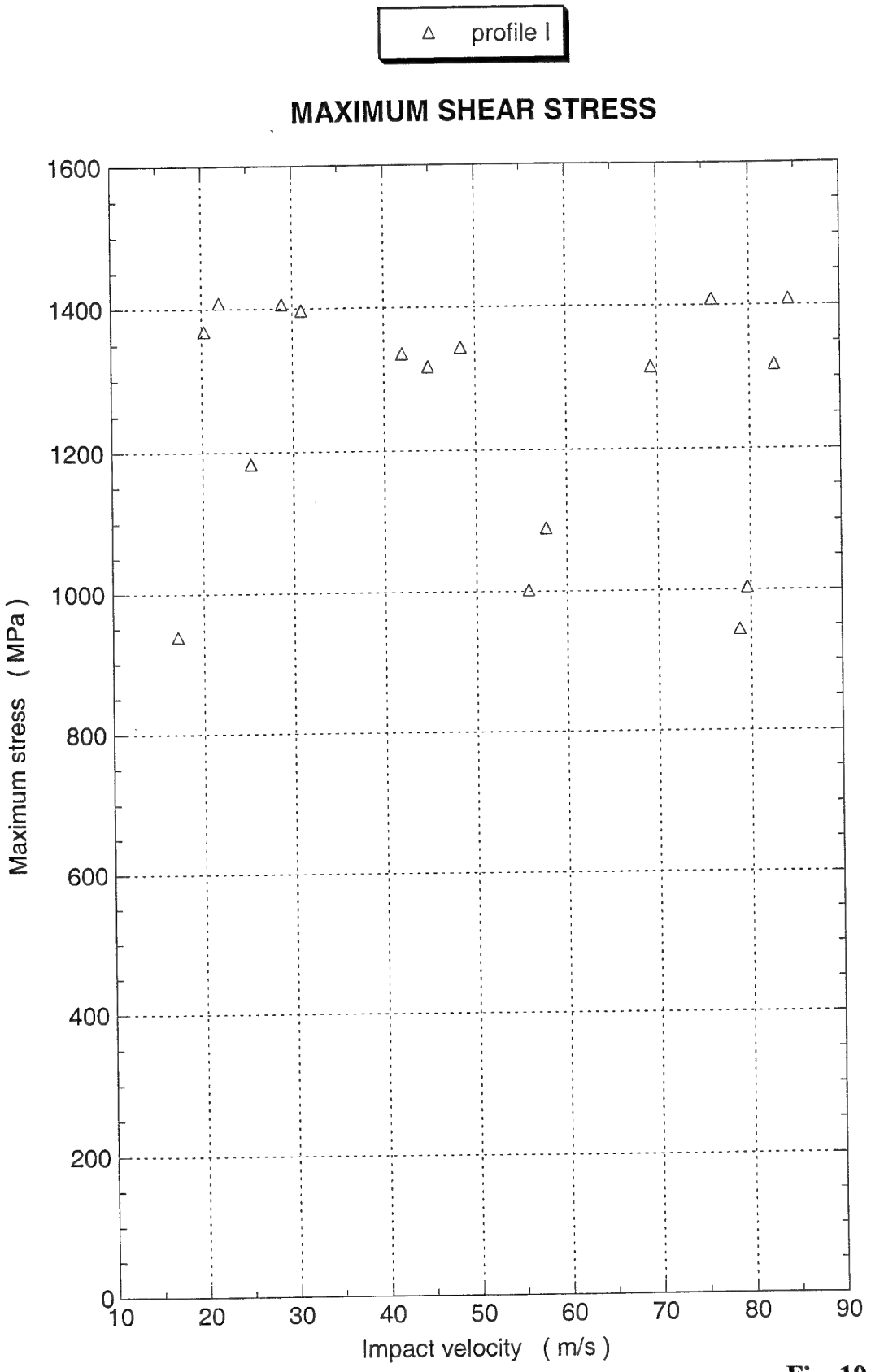
profile I
MAXIMUM SHEAR STRESS
Maximum stress (MPa)
1600
1400
1200
1000
800
600
400
200
0
10
20
30
40
50
60
70
80
90
Impact velocity (m/s)

Fig. 19

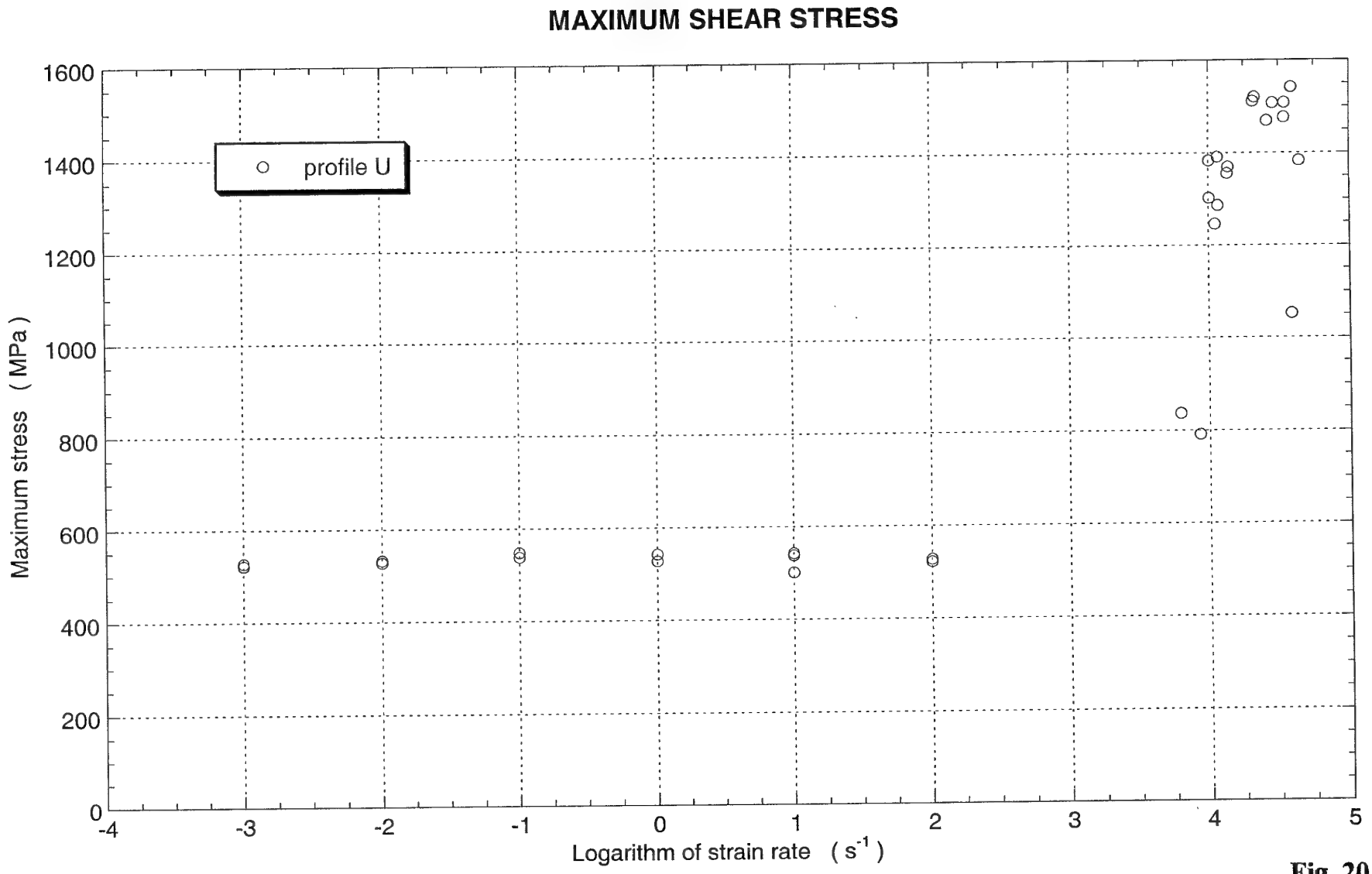
MAXIMUM SHEAR STRESS
profile U
Maximum stress (MPa)
Logarithm of strain rate (s-1)
1600
1400
1200
1000
800
600
400
200
0
-4
-3
-2
-1
0
1
2
3
4
5

Fig. 20

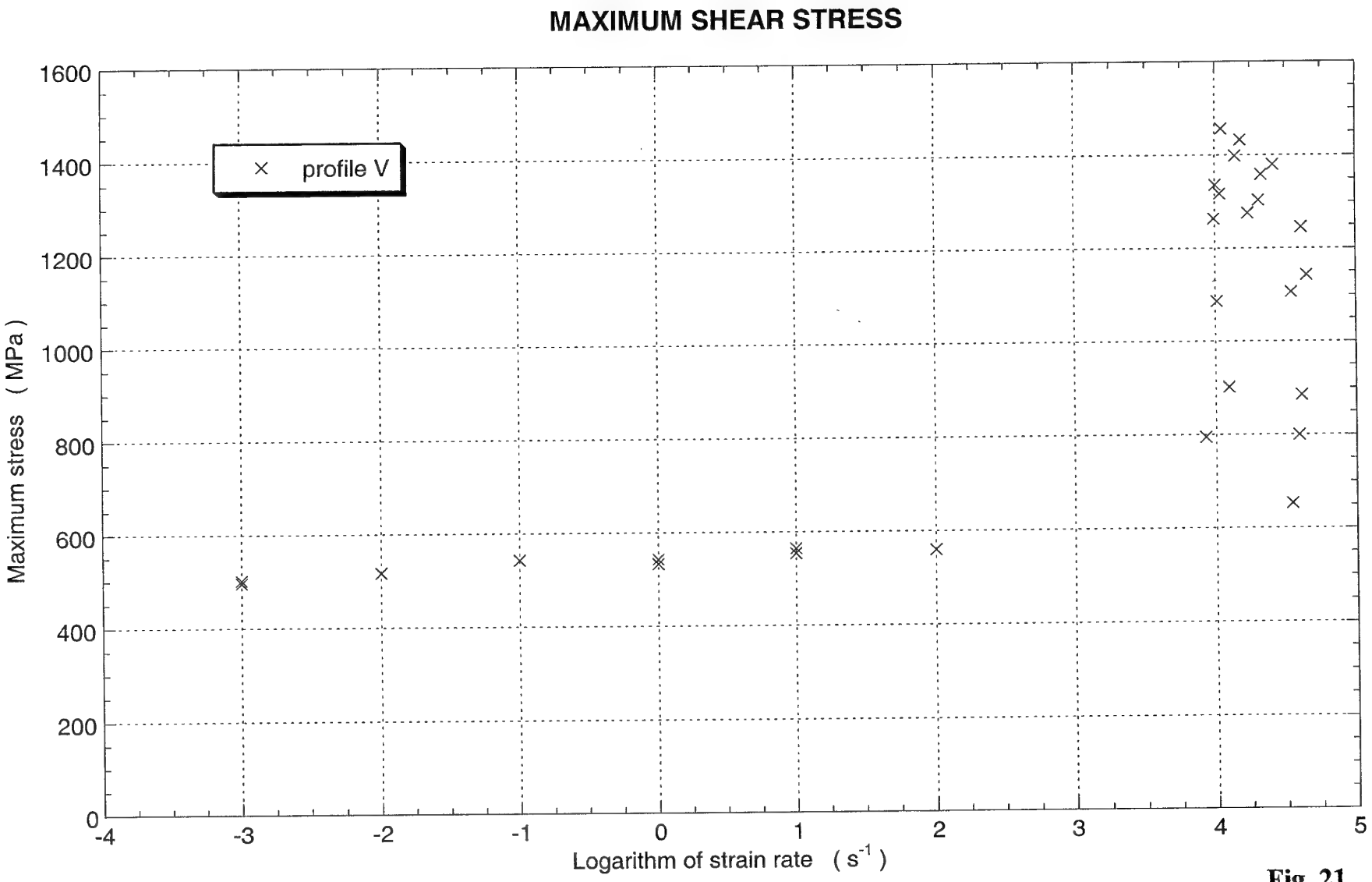
MAXIMUM SHEAR STRESS
profile V
Maximum stress (MPa)
Logarithm of strain rate (s-1)
1600
1400
1200
1000
800
600
400
200
0
-4
-3
-2
-1
0
1
2
3
4
5

Fig. 21

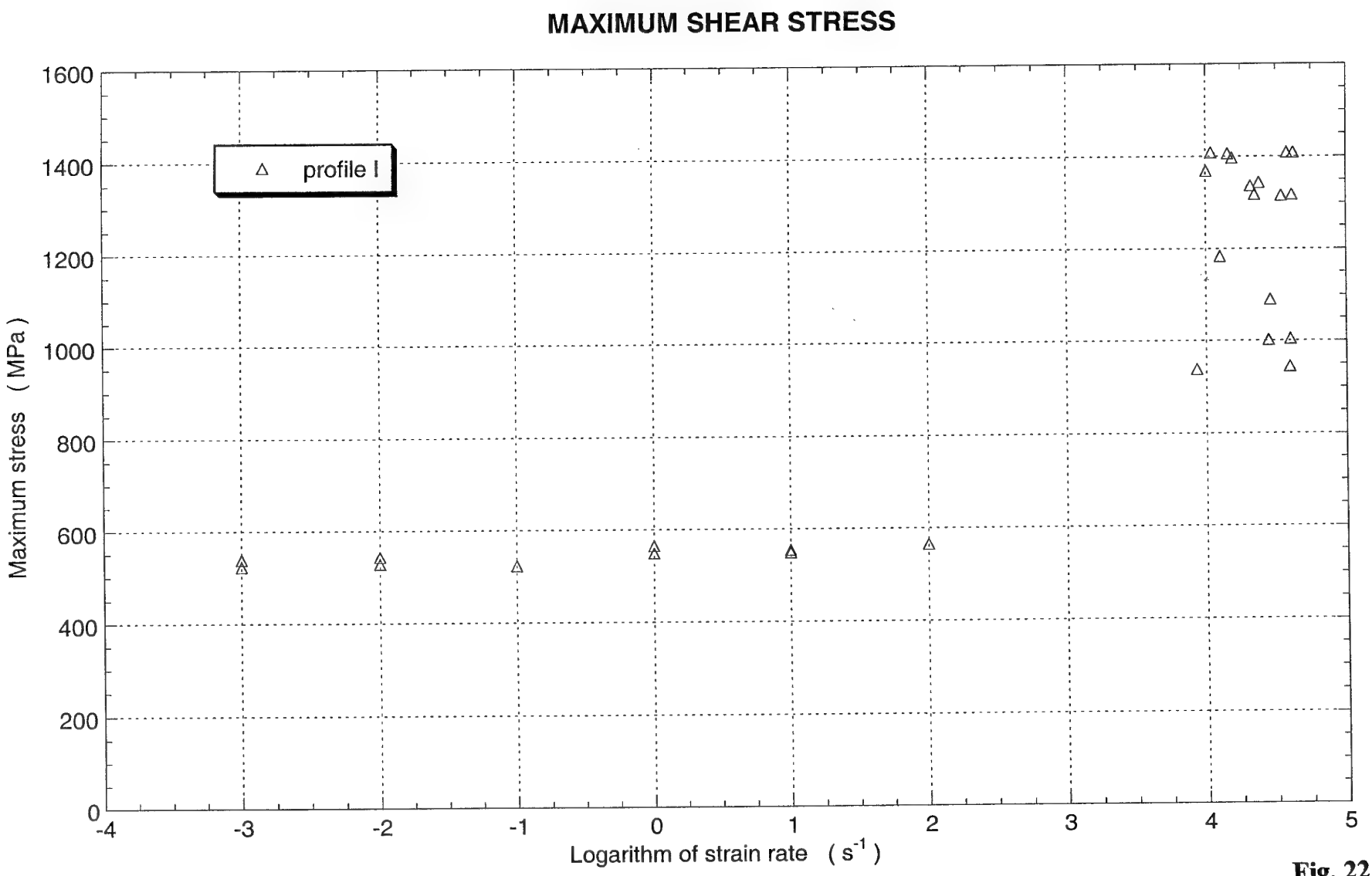
MAXIMUM SHEAR STRESS
profile I
Maximum stress (MPa)
Logarithm of strain rate (s-1)
1600
1400
1200
1000
800
600
400
200
0
-4
-3
-2
-1
0
1
2
3
4
5

Fig. 22

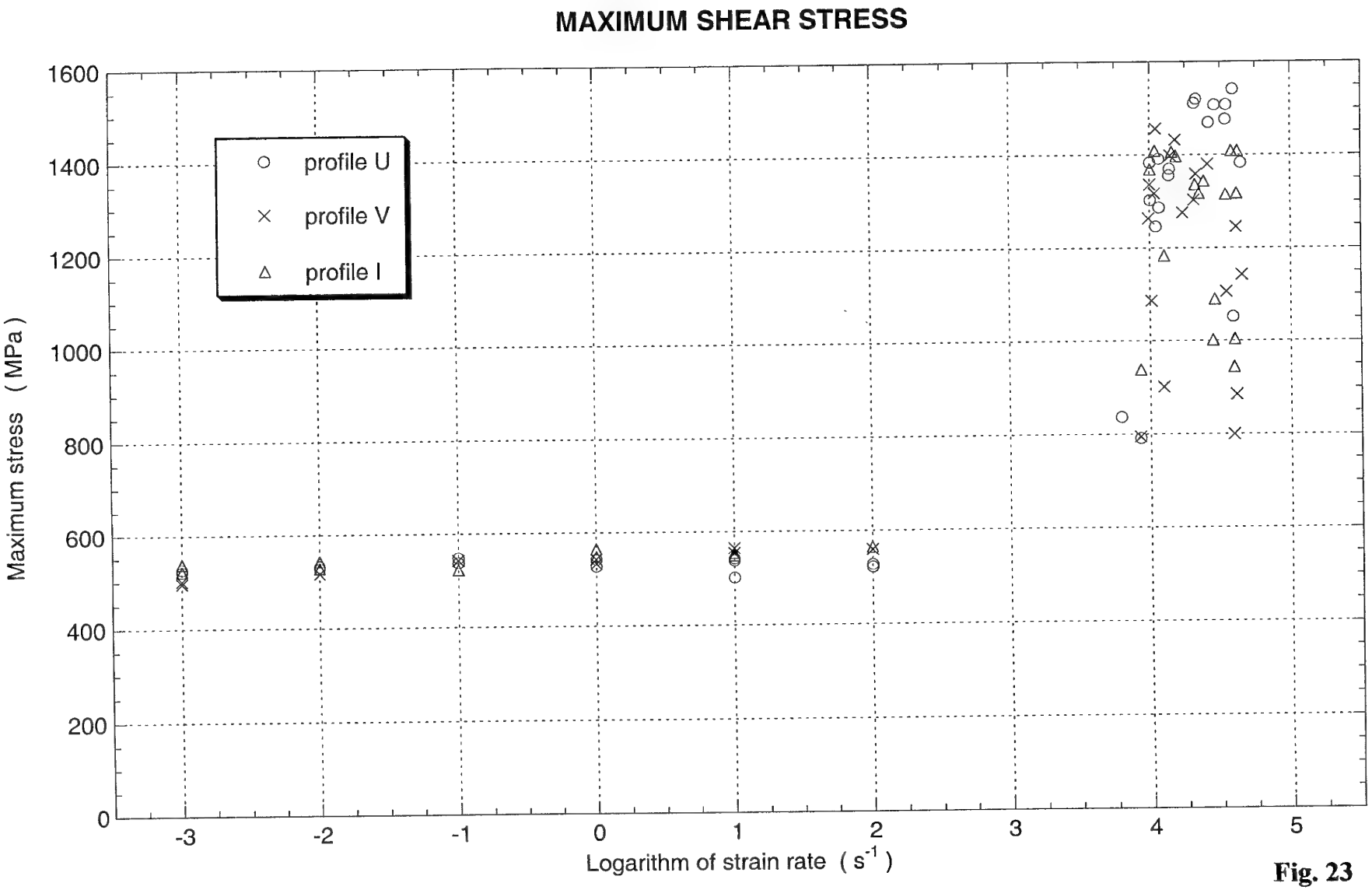
MAXIMUM SHEAR STRESS
profile U
profile V
profile I
Maximum stress (MPa)
Logarithm of strain rate (s-1)
1600
1400
1200
1000
800
600
400
200
0
-3
-2
-1
0
1
2
3
4
5

Fig. 23

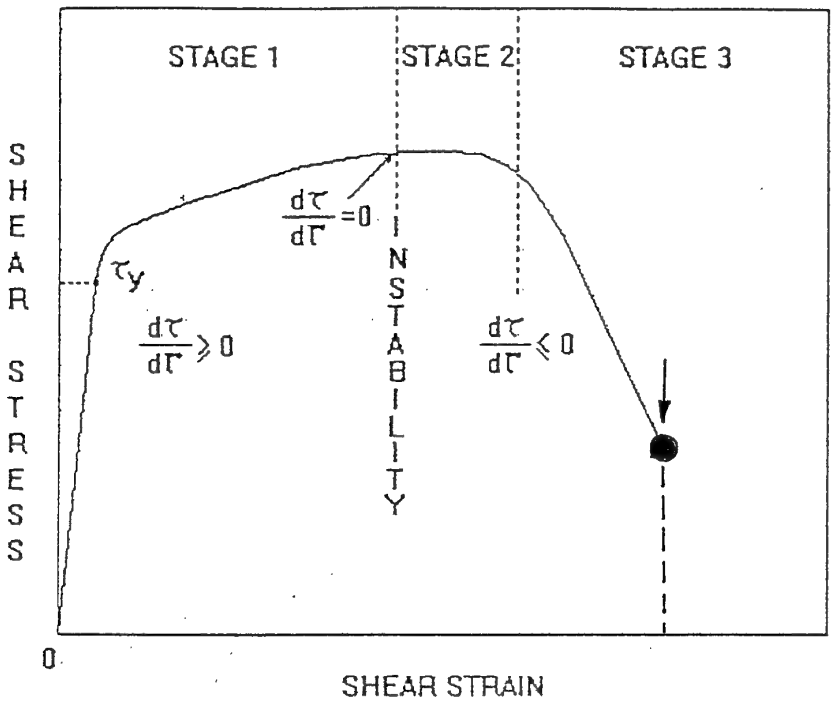
STAGE 1
STAGE 2
STAGE 3
SHEAR STRESS
$\frac{d\tau}{d\Gamma}=0$
τ_y
$\frac{d\tau}{d\Gamma}\geqslant 0$
INSTABILITY
$\frac{d\tau}{d\Gamma}\leqslant 0$
0
SHEAR STRAIN

Fig. 24

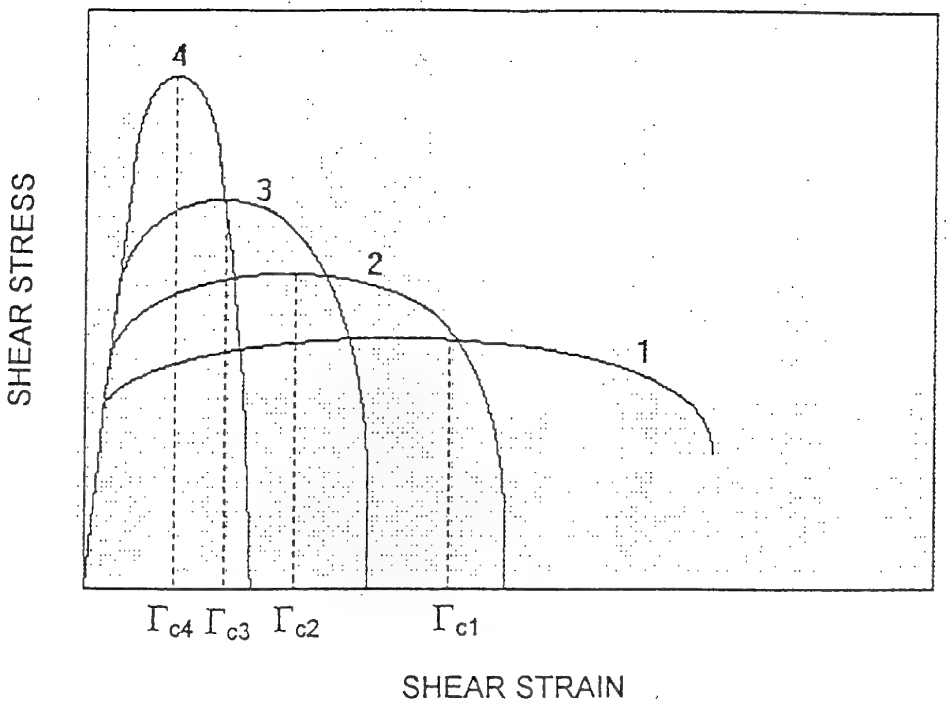
SHEAR STRESS
4
3
2
1
Γ_{c4} Γ_{c3} Γ_{c2} Γ_{c1}
SHEAR STRAIN

Fig. 25

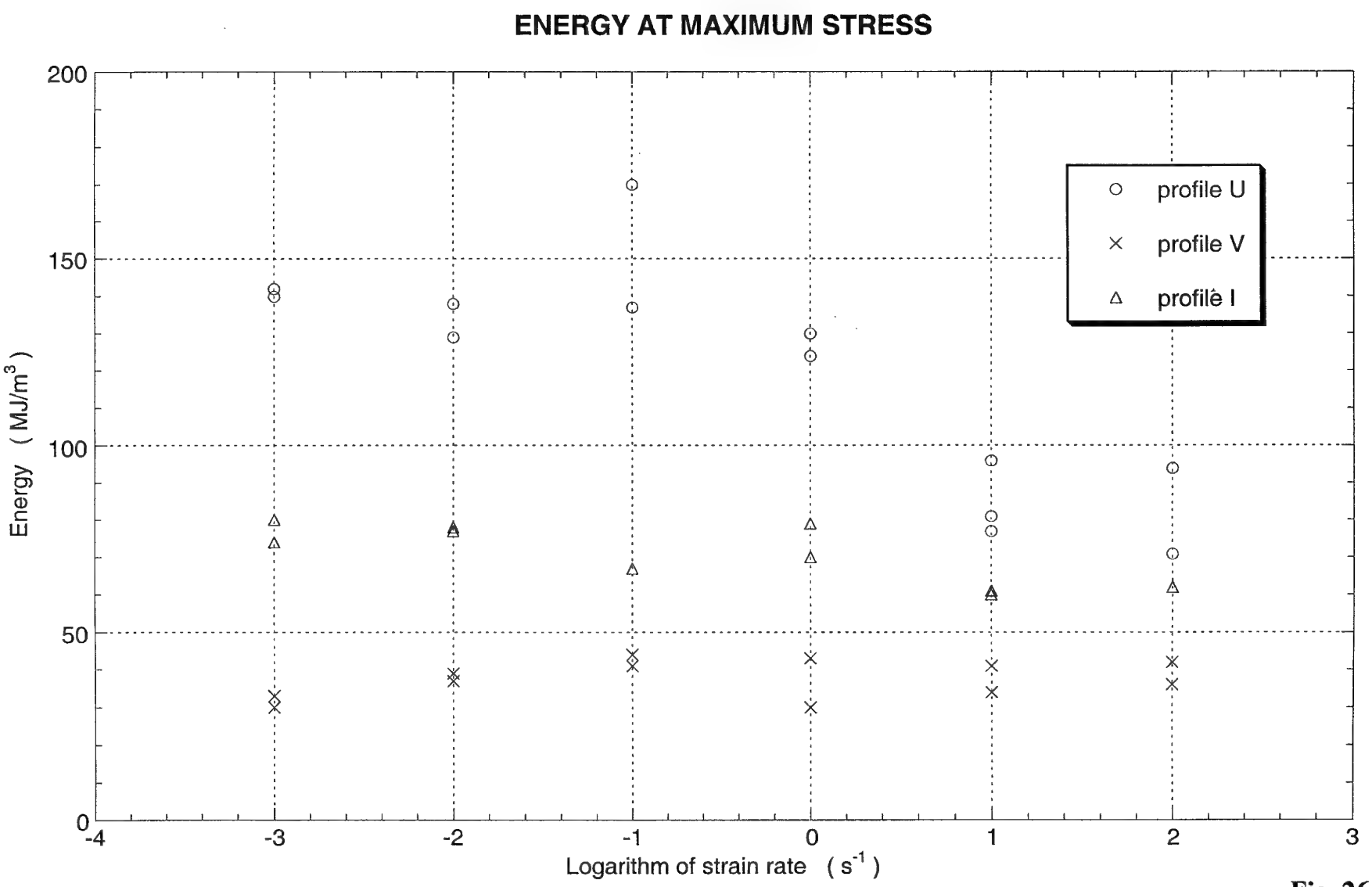
ENERGY AT MAXIMUM STRESS
200
150
100
50
0
Energy (MJ/m3)
-4
-3
-2
-1
0
1
2
3
Logarithm of strain rate (s-1)
profile U
profile V
profile I

Fig. 26

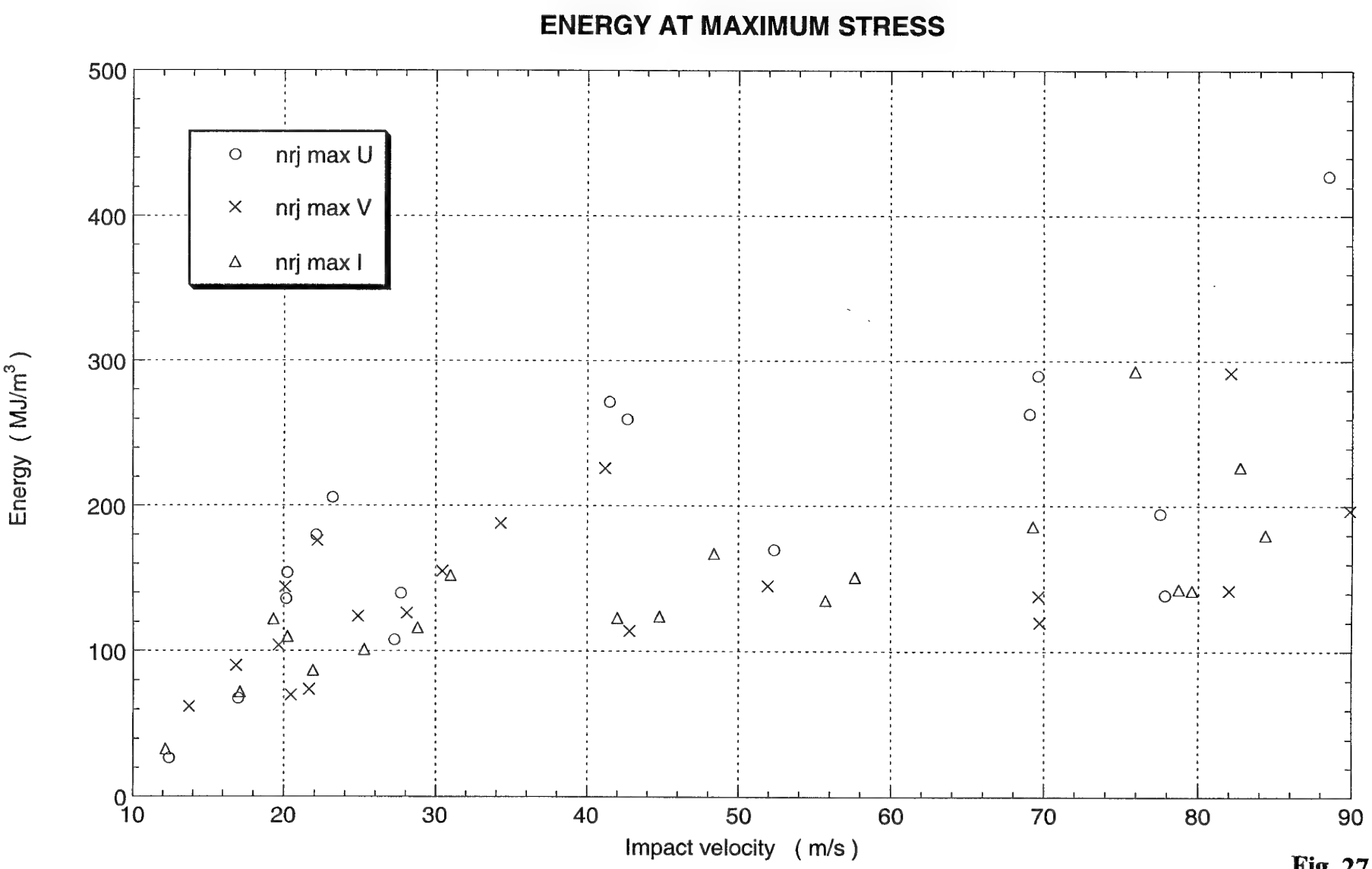
ENERGY AT MAXIMUM STRESS
nrj max U
nrj max V
nrj max I
Energy (MJ/m3)
Impact velocity (m/s)
0
100
200
300
400
500
10
20
30
40
50
60
70
80
90

Fig. 27

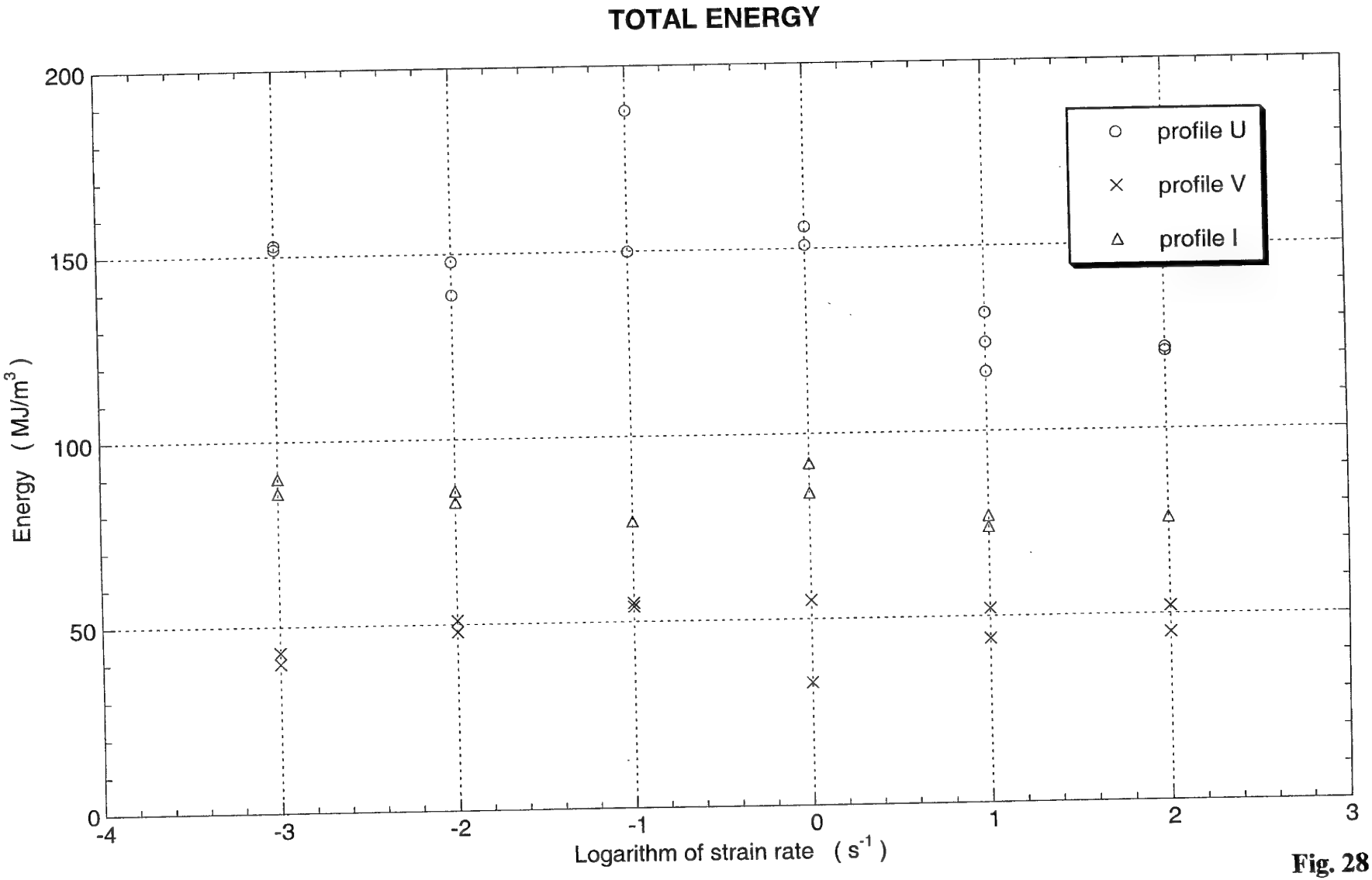
TOTAL ENERGY
200
150
100
50
0
-4
-3
-2
-1
0
1
2
3
Energy (MJ/m^3)
Logarithm of strain rate (s^{-1})
profile U
profile V
profile I

Fig. 28

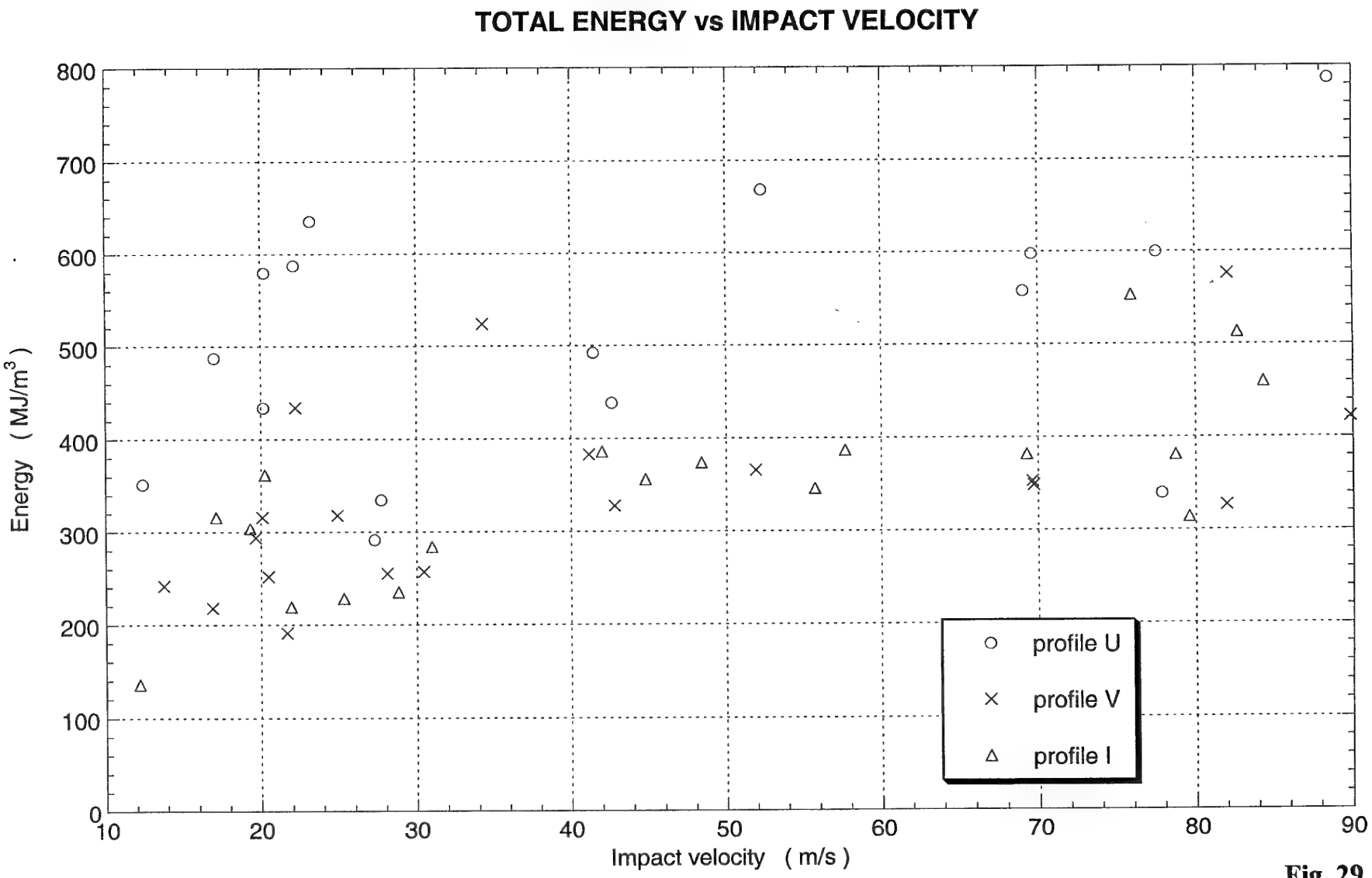
TOTAL ENERGY vs IMPACT VELOCITY
Energy (MJ/m3)
Impact velocity (m/s)
0
100
200
300
400
500
600
700
800
10
20
30
40
50
60
70
80
90
profile U
profile V
profile I

Fig. 29

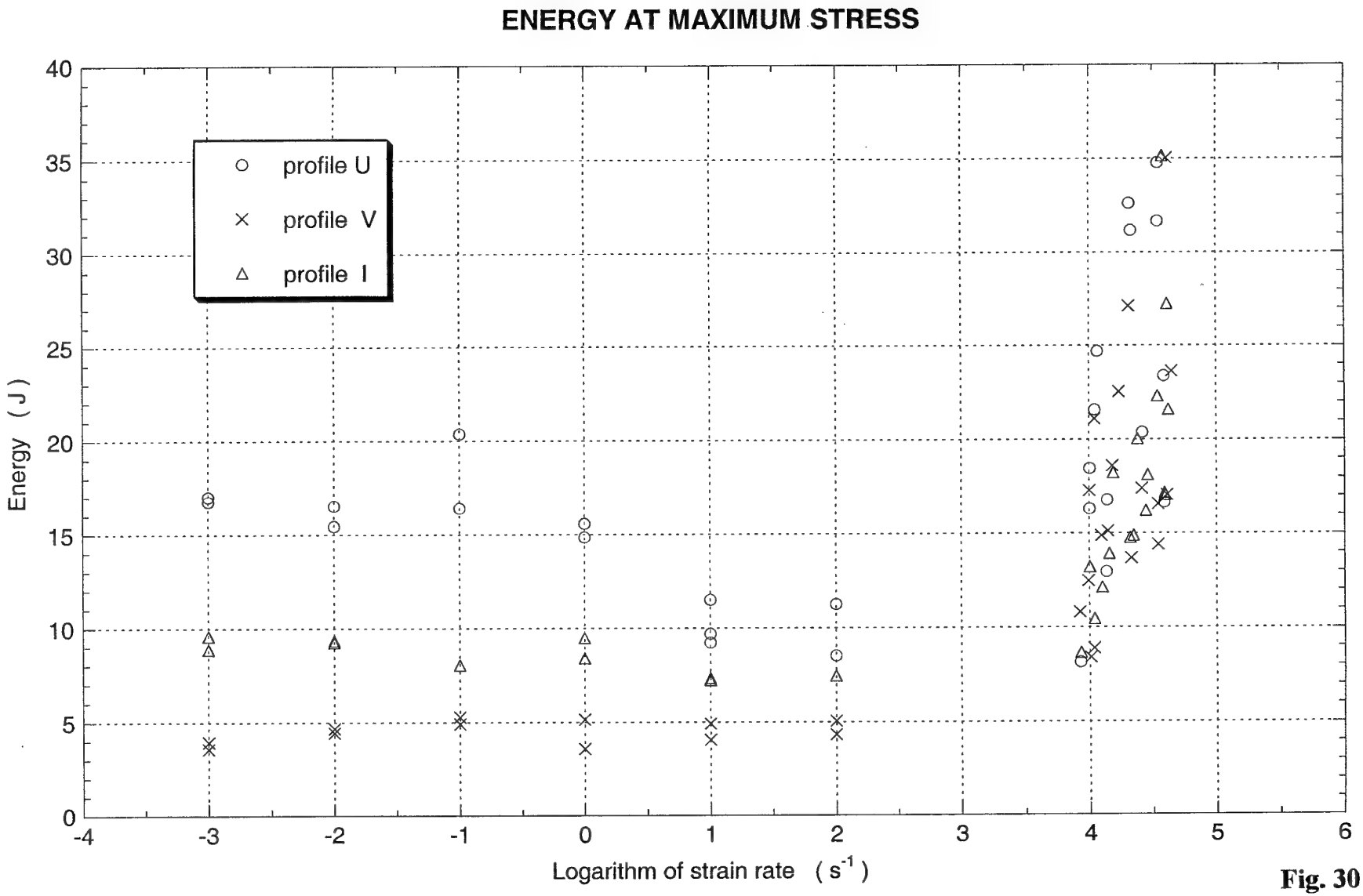
ENERGY AT MAXIMUM STRESS
profile U
profile V
profile I
Energy (J)
Logarithm of strain rate (s-1)
0
5
10
15
20
25
30
35
40
-4
-3
-2
-1
0
1
2
3
4
5
6

Fig. 30

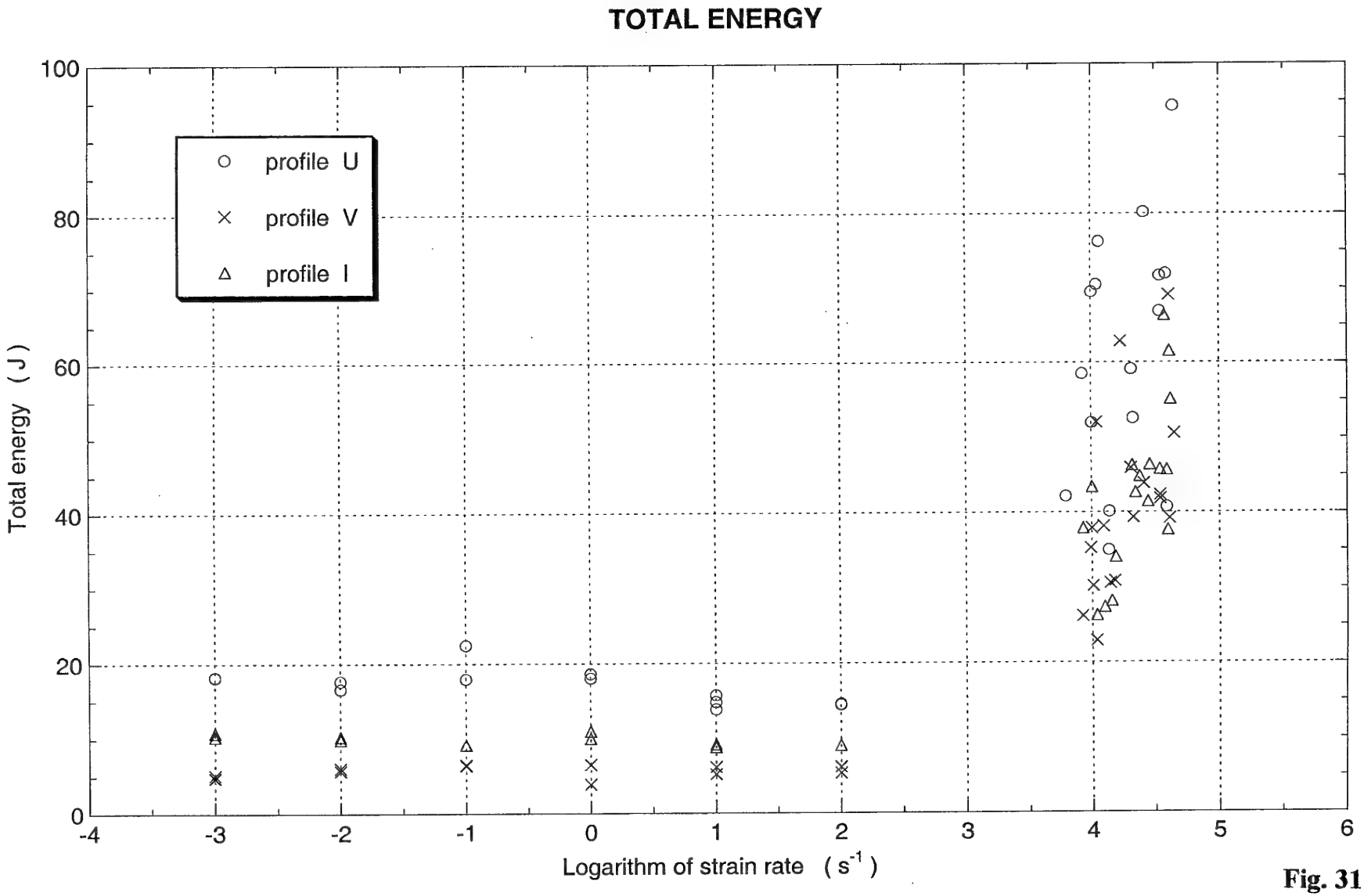
TOTAL ENERGY
profile U
profile V
profile I
Total energy (J)
Logarithm of strain rate (s-1)
100
80
60
40
20
0
-4
-3
-2
-1
0
1
2
3
4
5
6

Fig. 31

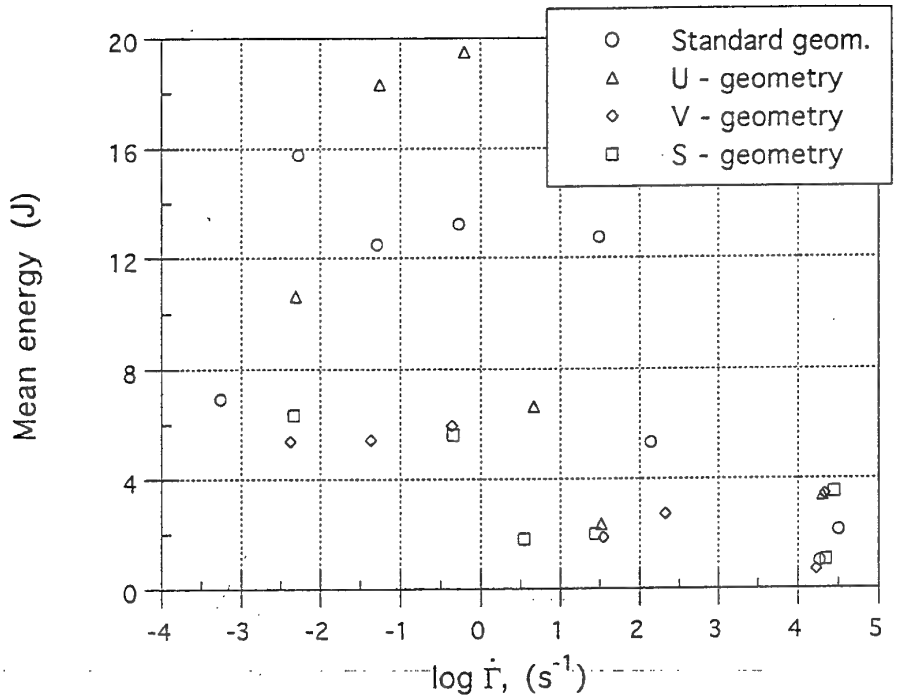
Standard geom.
U - geometry
V - geometry
S - geometry
Mean energy (J)
log Γ̇, (s-1)
20
16
12
8
4
0
-4
-3
-2
-1
0
1
2
3
4
5

Fig. 32

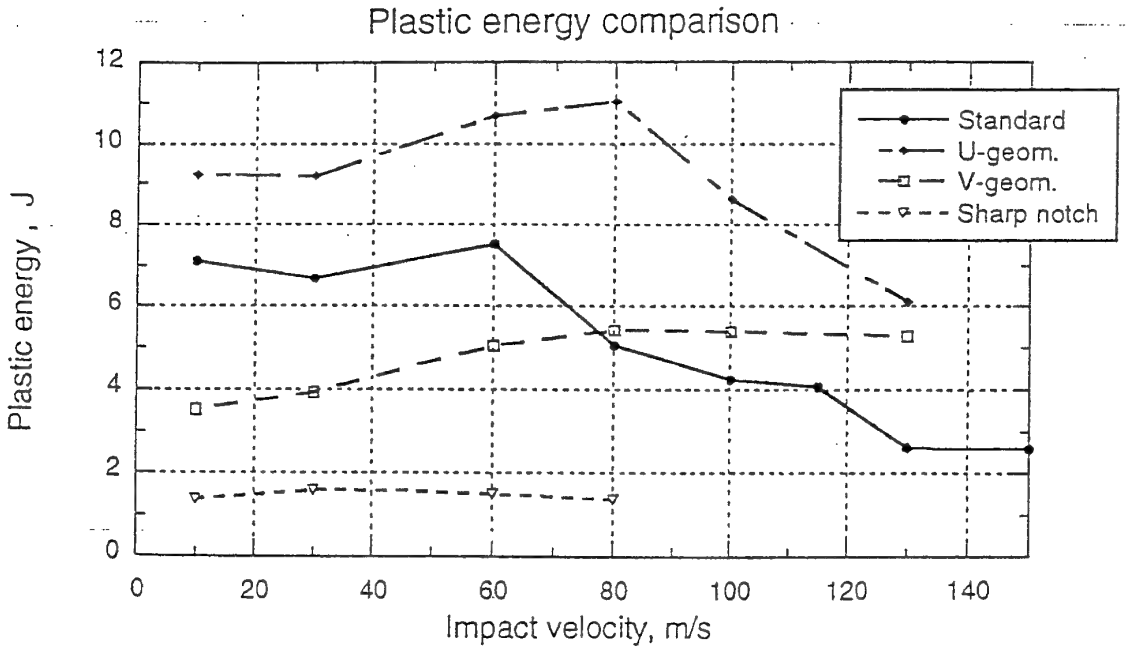
Plastic energy comparison
Standard
U-geom.
V-geom.
Sharp notch
Plastic energy , J
Impact velocity, m/s
12
10
8
6
4
2
0
0
20
40
60
80
100
120
140

Fig. 33

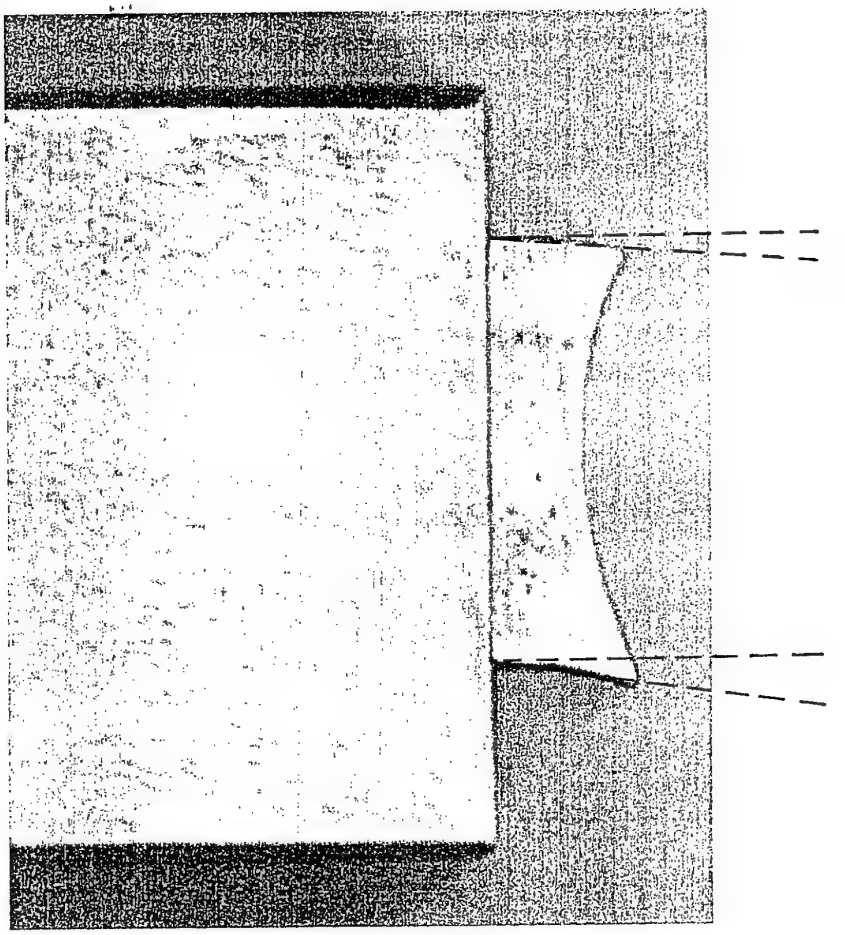

Fig. 34

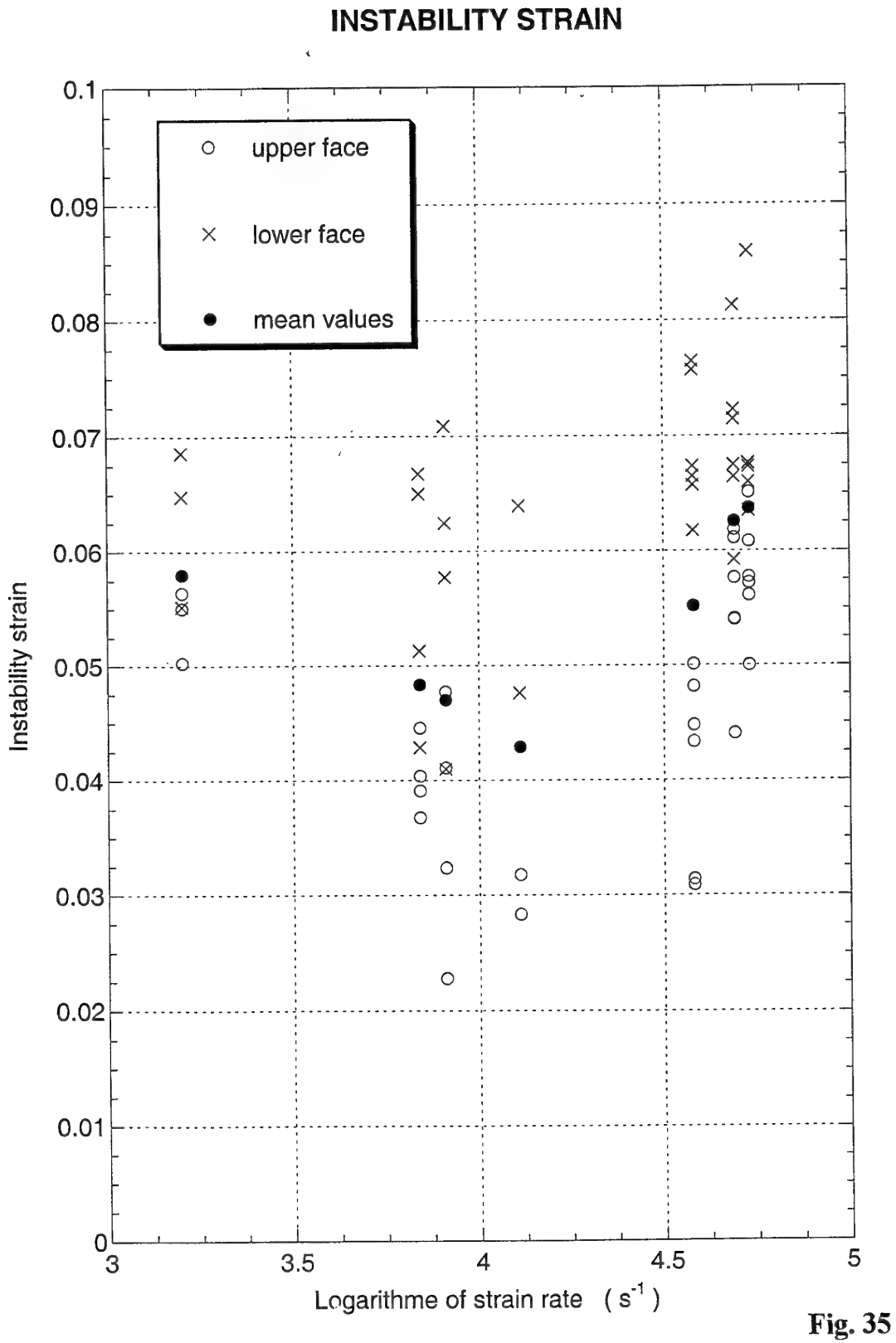
INSTABILITY STRAIN
upper face
lower face
mean values
Instability strain
0.1
0.09
0.08
0.07
0.06
0.05
0.04
0.03
0.02
0.01
0
3
3.5
4
4.5
5
Logarithme of strain rate (s-1)

Fig. 35

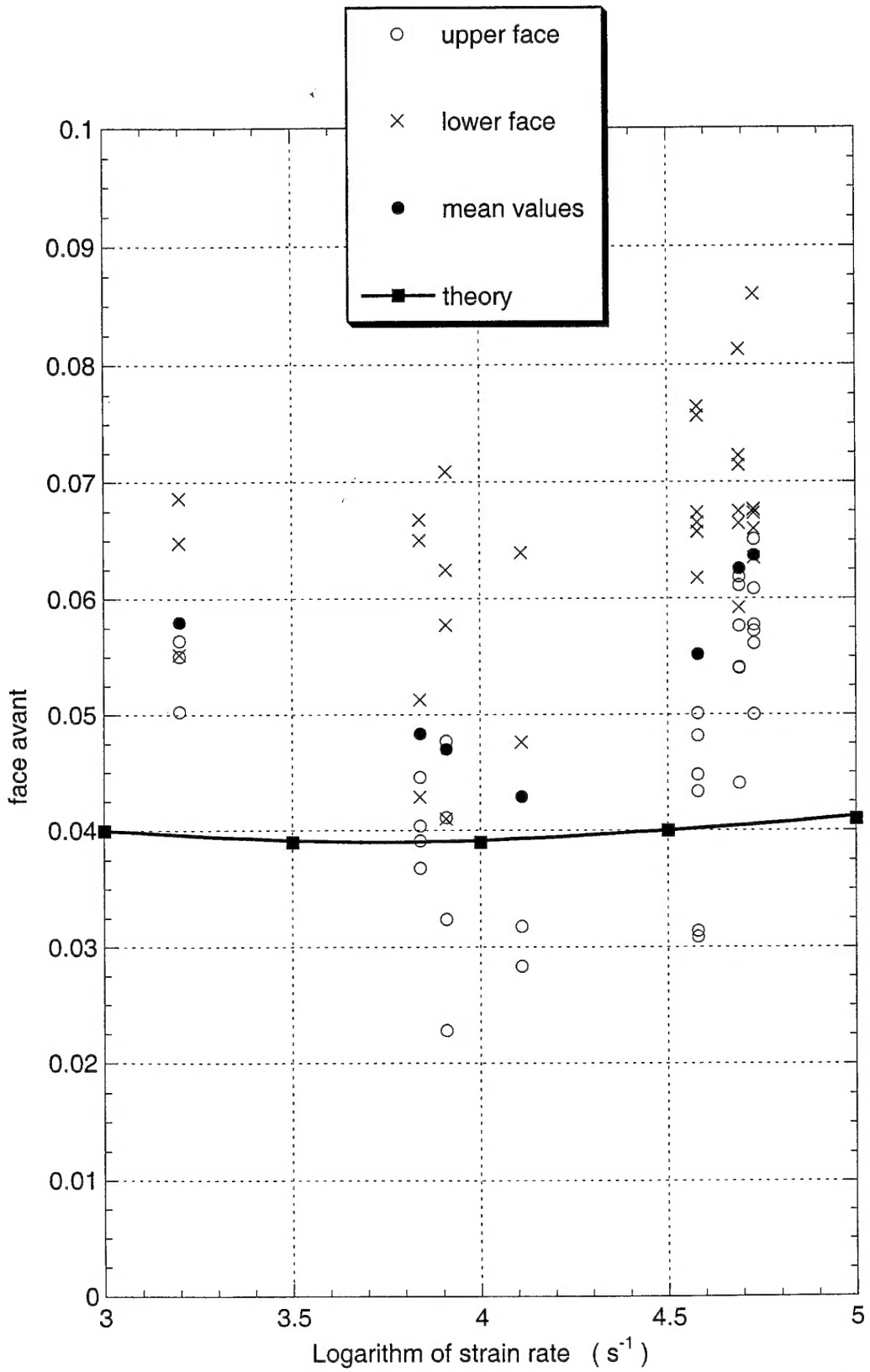
INSTABILITY STRAIN
upper face
lower face
mean values
theory
face avant
0.1
0.09
0.08
0.07
0.06
0.05
0.04
0.03
0.02
0.01
0
3
3.5
4
4.5
5
Logarithm of strain rate (s-1)

Fig. 36

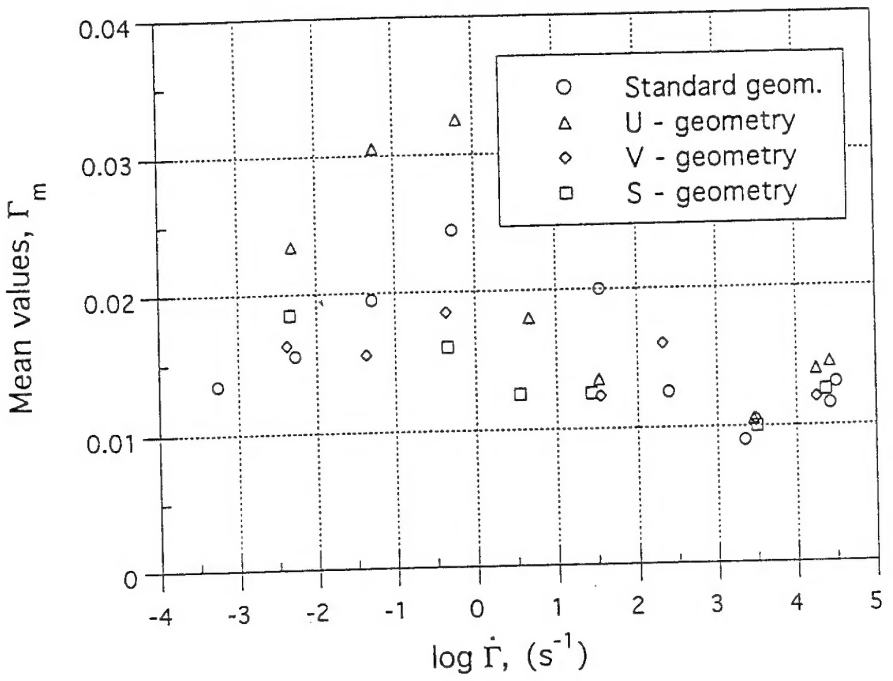
Standard geom.
U - geometry
V - geometry
S - geometry
Mean values, Γ_m
log $\dot{\Gamma}$, (s^{-1})
0.04
0.03
0.02
0.01
0
-4
-3
-2
-1
0
1
2
3
4
5

Fig. 37

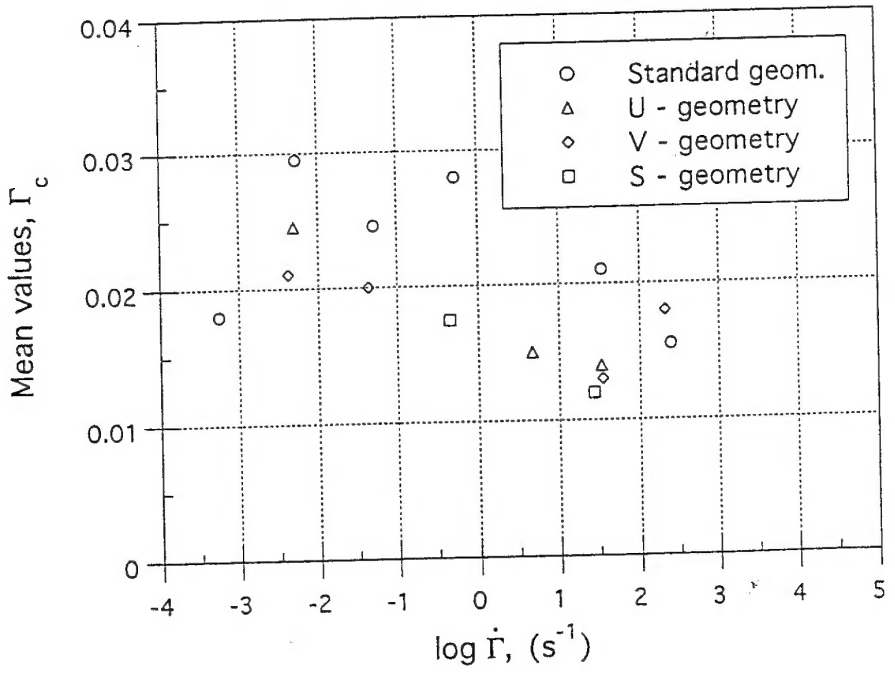
Standard geom.
U - geometry
V - geometry
S - geometry
Mean values, Γ_c
log $\dot{\Gamma}$, (s^{-1})
0.04
0.03
0.02
0.01
0
-4
-3
-2
-1
0
1
2
3
4
5

Fig. 38

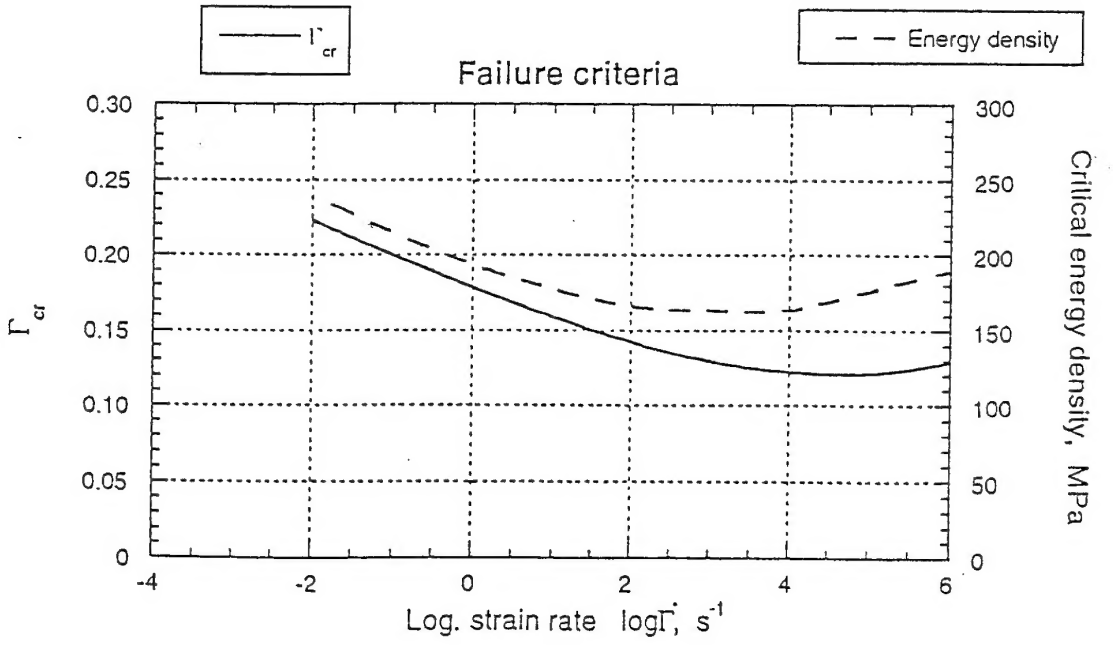
Failure criteria
Energy density
Γcr
0.30
0.25
0.20
0.15
0.10
0.05
0
300
250
200
150
100
50
0
-4
-2
0
2
4
6
Log. strain rate logΓ̇, s-1
Crillcal energy density, MPa

Fig. 39

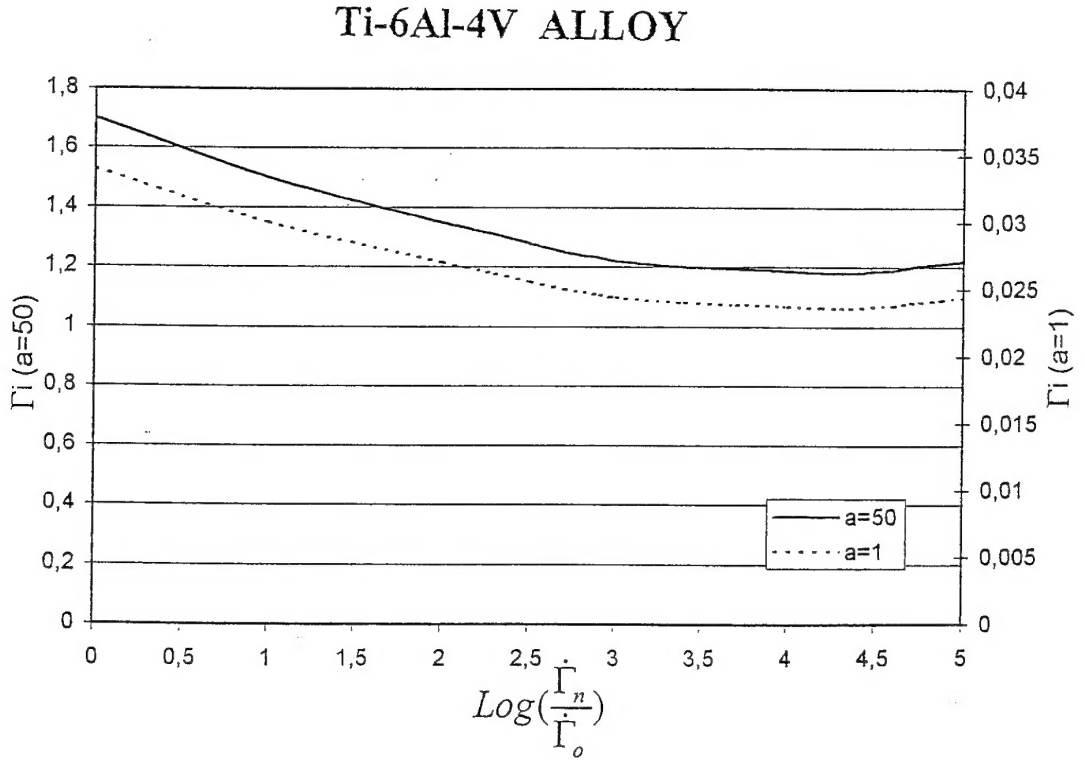
Ti-6Al-4V ALLOY
Γi (a=50)
Γi (a=1)
1,8
1,6
1,4
1,2
1
0,8
0,6
0,4
0,2
0
0,04
0,035
0,03
0,025
0,02
0,015
0,01
0,005
0
0
0,5
1
1,5
2
2,5
3
3,5
4
4,5
5
a=50
a=1
Log(Γ̇n / Γ̇o)

Fig. 40

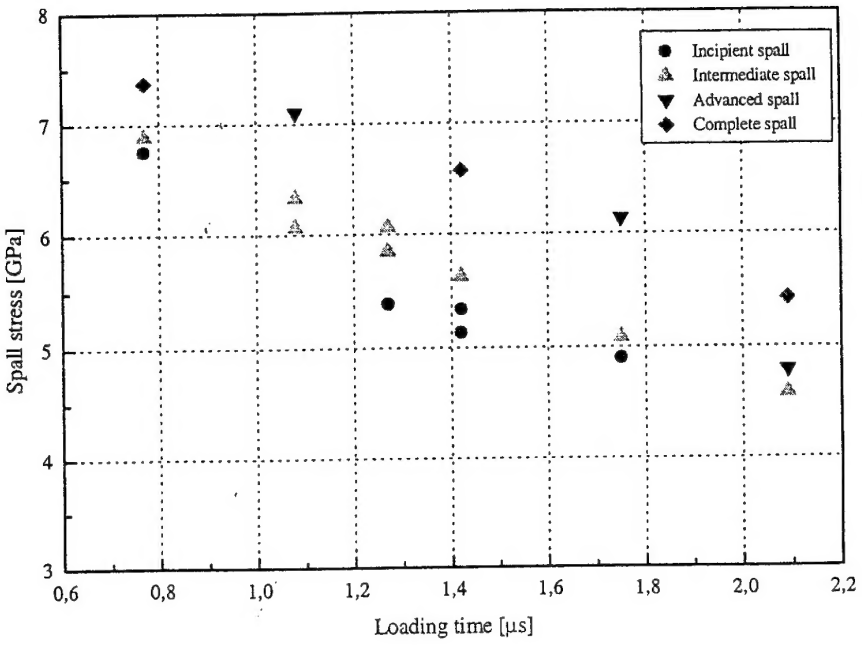
Incipient spall
Intermediate spall
Advanced spall
Complete spall
Spall stress [GPa]
Loading time [μs]
8
7
6
5
4
3
0,6
0,8
1,0
1,2
1,4
1,6
1,8
2,0
2,2

Fig. 41

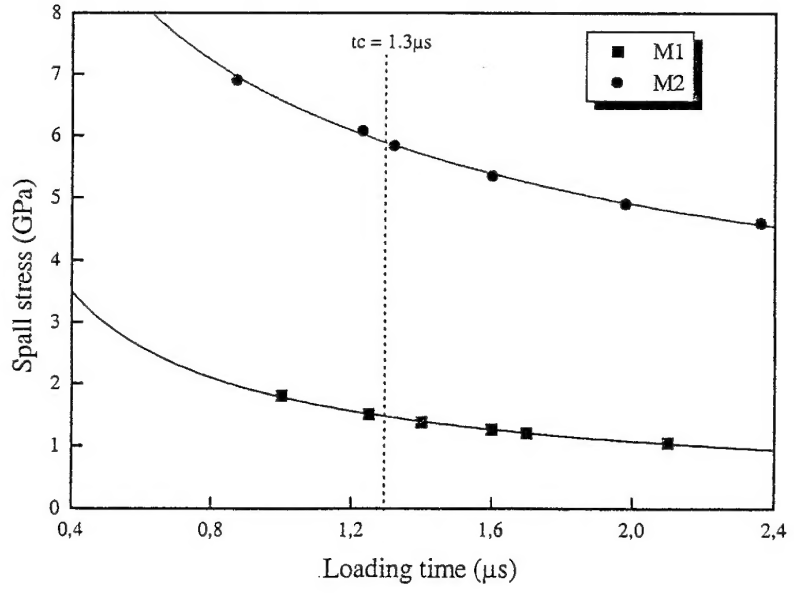
tc = 1.3μs
M1
M2
Spall stress (GPa)
Loading time (μs)
8
7
6
5
4
3
2
1
0
0,4
0,8
1,2
1,6
2,0
2,4

Fig. 42